

January 5, 2016

Dr Jatin Kala
Topical Editor
Geoscientific Model Development Discussions

Dear Dr Kala.

Re: The GEWEX LandFlux project: evaluation of model evaporation using tower-based and globally-gridded forcing data by McCabe et al. (2015).

Thank you for your update regarding the status of our manuscript. We are pleased to hear that the paper is nearing acceptance into Geoscientific Model Development, subject to the minor revisions you have outlined. I have addressed the requested changes through additional text as requested, which is referenced below for your consideration. The changes have been made as follows (new text in red):

Addition to Introduction, Page 6, Line 144: “While establishing a baseline level of performance at the tower scale is important, understanding the impact of using the large-scale globally-gridded forcing that will ultimately drive global products is key. **Indeed, undertaking a parallel assessment between the tower and grid scales, while imposing consistency in the forcing data and sampling locations used, allows for a much greater understanding of model response than can be achieved through either assessment in isolation: an important extension upon recent tower-only analyses, such as Ershadi et al. (2014) and related contributions.**”

Addition to the Discussion, Page 29, Line 783: “These results **are consistent with** previous findings **undertaken across a smaller number of towers and biome and climate types**, that any one modelling approach is incapable of accurately reflecting the range of flux responses occurring across diverse landscapes (Ershadi et al., 2014; Ershadi et al., 2015).”

Changes to the structure of the Introduction: The adjusted introductory paragraph (above) has now been linked directly to the original paragraph (where the Ershadi papers are discussed) so that the reader can clearly relate the differences of the present contribution to these earlier works. They were previously separated paragraphs. The discussion of the WACMOS-ET work has now been moved immediately below this.

With these small changes, I agree that the manuscript is now a stronger contribution, allowing the reader to clearly identify the important contribution of our work. If there are any further changes required to the manuscript, please do not hesitate to contact me at your convenience.

Best wishes,



Dr Matthew McCabe
Professor of Hydrology and Land Observation
King Abdullah University of Science and Technology

1 **The GEWEX LandFlux project: evaluation of model evaporation using tower-**
2 **based and globally-gridded forcing data**

3

4 **Matthew F. McCabe^{1*}, Ali Ershadi¹, Carlos Jimenez², Diego G. Miralles³, Dominik Michel⁴**
5 **and Eric F. Wood⁵**

6 [1] {Division of Biological and Environmental Sciences and Engineering, King Abdullah University
7 of Science and Technology, Thuwal, Saudi Arabia}

8 [2] {Estellus, Paris, France}

9 [3] {Department of Earth Sciences, VU University Amsterdam, Amsterdam, The Netherlands}

10 [4] {Institute for Atmospheric and Climate Sciences, ETH Zurich, Zurich, Switzerland}

11 [5] {Department of Civil and Environmental Engineering, Princeton University, Princeton, United
12 States of America}

13 * Correspondence to: matthew.mccabe@kaust.edu.sa

14

15 **Abstract**

16 Determining the spatial distribution and temporal development of evaporation at regional and
17 global scales is required to improve our understanding of the coupled water and energy cycles
18 and to better monitor any changes in observed trends and variability of linked hydrological
19 processes. With recent international efforts guiding the development of long-term and globally
20 distributed flux estimates, continued product assessments are required to inform upon the
21 selection of suitable model structures and also to establish the appropriateness of these multi-
22 model simulations for global application. In support of the objectives of the GEWEX LandFlux
23 project, four commonly used evaporation models are evaluated against data from tower-based
24 eddy-covariance observations, distributed across a range of biomes and climate zones. The
25 selected schemes include the Surface Energy Balance System (SEBS) approach, the Priestley-
26 Taylor Jet Propulsion Laboratory (PT-JPL) model, the Penman-Monteith based Mu model (PM-

27 Mu) and the Global Land Evaporation Amsterdam Model (GLEAM). Here we seek to examine
28 the fidelity of global evaporation simulations by examining the multi-model response to varying
29 sources of forcing data. To do this, we perform parallel and collocated model simulations using
30 tower-based data together with a global-scale grid-based forcing product. Through quantifying
31 the multi-model response to high-quality tower data, a better understanding of the subsequent
32 model response to the coarse-scale globally gridded data that underlies the LandFlux product
33 can be obtained, while also providing a relative evaluation and assessment of model
34 performance.

35 Using surface flux observations from forty-five globally distributed eddy-covariance stations as
36 independent metrics of performance, the tower-based analysis indicated that PT-JPL provided
37 the highest overall statistical performance (0.72 ; 61 W.m^{-2} ; 0.65), followed closely by GLEAM
38 (0.68 ; 64 W.m^{-2} ; 0.62), with values in parenthesis representing the R^2 , $RMSE$ and Nash-Sutcliffe
39 Efficiency (NSE), respectively. PM-Mu (0.51 ; 78 W.m^{-2} ; 0.45) tended to underestimate fluxes,
40 while SEBS (0.72 ; 101 W.m^{-2} ; 0.24) overestimated values relative to observations. A focused
41 analysis across specific biome types and climate zones showed considerable variability in the
42 performance of all models, with no single model consistently able to outperform any other.
43 Results also indicated that the global gridded data tended to reduce the performance for all of
44 the studied models when compared to the tower data, likely a response to scale mismatch and
45 issues related to forcing quality. Rather than relying on any single model simulation, the spatial
46 and temporal variability at both the tower- and grid-scale highlighted the potential benefits of
47 developing an ensemble or blended evaporation product for global scale LandFlux applications.
48 Challenges related to the robust assessment of the LandFlux product are also discussed.

49

50 1 Introduction

51 Characterizing the exchange of water between the land surface and the atmosphere is a topic
52 of multi-disciplinary interest, as the processes that comprise this dynamic cycling of water
53 determine the spatial and temporal variability of hydrological responses across local and global
54 scales. In recent years, there has been significant progress in the development of regional and

Matthew McCabe 5/1/2016 10:41 AM

Deleted: (

Matthew McCabe 5/1/2016 10:41 AM

Deleted:)

57 global datasets based largely on remote sensing retrievals. These data have provided a wealth
58 of spatially and temporally varying information across a range of Earth system processes,
59 including soil moisture (Liu et al., 2011a), vegetation change (Tucker et al., 2005; Liu et al.,
60 2011b; Liu et al., 2013), groundwater (Famiglietti et al., 2011; Richey et al., 2015) and
61 precipitation (Huffman et al., 1995; Nesbitt et al., 2004), enabling a capacity to enhance our
62 understanding and description of regional- and global-scale water cycles and their spatial and
63 temporal variability. While evaporation represents the key process returning the Earth's surface
64 water to the overlying atmosphere and provides the linking mechanism between the water and
65 energy cycles, it is only in relatively recent times that effort has been directed towards the
66 development of global products (Mu et al., 2007; Fisher et al., 2008; Vinukollu et al., 2011a).

67 To address this observation limitation, a number of evaporation modelling approaches have
68 been developed over the past few years to enable estimation at scales beyond the field, using
69 satellite remote sensing (Sheffield et al., 2010; Miralles et al., 2011a) and other data sources
70 (Douville et al., 2013). The models tend to differ in their level of empiricism and in the desired
71 scale of application, with some exclusively developed for farm-scale operation and requiring
72 local calibration (Bastiaanssen et al., 1998; Allen et al., 2007). Others have been developed for
73 broader scale application and are built on physical relationships describing the water and
74 energy transfer at the land surface (Norman et al., 1995; Su, 2002; Fisher et al., 2008; Miralles
75 et al., 2011a). While traditional applications of evaporation estimates have been directed
76 towards agricultural monitoring (Allen, 2000), catchment water budgets and basin-scale water
77 management (Kustas et al., 1994; Granger, 2000), more recent applications of evaporation
78 products have included detection and prediction of heatwaves (Hirschi et al., 2011; Miralles et
79 al., 2014a), droughts (Mu et al., 2012; Otkin et al., 2014) and in resolving the likely contribution
80 of human-induced climate change on such events (Greve et al., 2014).

81 Despite the importance of understanding the magnitude and spatial and temporal variability of
82 evaporation, the availability of long-term products required to do this are rather limited.
83 Characterizing the long-term trends and variability in independent observations of the Earth's
84 coupled water and energy cycles is a key objective of the World Climate Research Programmes
85 (WCRP) Global Energy and Water Cycle Exchanges (GEWEX) project. Towards this task, the

86 GEWEX Data and Assessments Panels (GDAP) LandFlux project has coordinated two interrelated
87 research efforts that seek to: i) intercompare long-term gridded surface flux data sets and
88 identify their skill and reliability (i.e. product-benchmarking), and ii) simulate and intercompare
89 evaporation models to identify algorithms appropriate for developing a global flux product (i.e.
90 model-benchmarking). In one of the first global-scale product assessments, Jiménez et al.
91 (2011) examined twelve evaporation products obtained from satellite-based, reanalyses and
92 off-line [land surface model \(LSM\)](#) simulations for a 3 year period (1993-1995), identifying large
93 correlations between the products, similarity in their spatial distributions, as well as large
94 absolute differences in the annual average evaporation. A complementary investigation of the
95 inter-product differences was undertaken by Mueller et al. (2011), which included forty-one
96 global evaporation data sets across a range of satellite-based simulations, LSMs, Global
97 Circulation Models (GCMs), atmospheric reanalyses datasets, empirical up-scaling of eddy-
98 covariance measurements, as well as atmospheric water budget data sets. In that study,
99 Mueller et al. (2011) used seven years of monthly mean data for the period 1989-1995 and
100 found strong similarity in the absolute magnitude and spatial distribution of evaporation
101 amongst the products. More recently, Mueller et al. (2013) examined multi-annual trends and
102 variations in evaporation products from a range of diagnostic data sets, LSMs and reanalysis
103 products and showed consistency in inter-annual variations of evaporation products that
104 corresponded well with previous investigations (Jung et al., 2010).

105 These benchmarking studies provided a thorough (and much needed) assessment of available
106 global evaporation products and the varying approaches used to derive them. However,
107 evaluation of the models for their predictive skill was challenging due to inconsistencies in the
108 forcing data used to drive the models, as well as to the different parameterization schemes
109 employed. That is, the analysis was performed on the published evaporation output, rather
110 than re-running simulations from a common forcing dataset. In these benchmarking studies,
111 the evaporation data sets were also aggregated to similar spatial and temporal resolutions for a
112 common analysis period, to enable unbiased comparison. Uncertainties emerging from such
113 aggregations can often reduce the confidence in any [subsequent](#) model performance ranking.

114 One initial effort addressing this was the study of Vinukollu et al. (2011a), which used the

Matthew McCabe 5/1/2016 10:51 AM

Deleted: such

116 Surface Energy Balance System (SEBS) model (SEBS; Su, 2002), a two-source Penman-Monteith
117 scheme by Mu et al. (2007) and a three-source model based on parameterizing the Priestley-
118 Taylor model (PT-JPL) (Fisher et al., 2008) to estimate global evaporation for the period 2003-
119 2004. The Vinukollu et al. (2011a) analysis revealed that the modelled instantaneous
120 evaporation (coinciding with the time of satellite overpass) was in reasonable agreement with
121 locally-observed evaporation at twelve eddy-covariance towers across the United States, with
122 correlations ranging from 0.43 to 0.54. However, uncertainties resulting from scale mismatch
123 between satellite data and the validation tower footprint reduced the confidence and skill
124 ranking of the models. One of the unique aspects of the present study is that tower data are
125 consistent across all model simulations: that is, tower-bias is minimized, by ensuring that all
126 models are assessed against the same tower records. Further, even though sub-grid scale
127 variability is not explored here (since none of the models explicitly account for this), the tower-
128 to-grid scale analysis acts as a diagnostic of representativeness and point-to-pixel error.

129 Recently, Ershadi et al. (2014) examined a number of models including SEBS, PT-JPL, the
130 Advection-Aridity model of Brutsaert and Stricker (1979) and a single-source Penman-Monteith
131 (PM) model (Monteith, 1965), using a set of twenty flux towers distributed across a range of
132 biome types and climate zones to force the models with tower-based data directly. Based on
133 common forcing and considering overall results, the study found that PT-JPL was the best
134 performing model, followed by SEBS, PM and Advection-Aridity. In a related contribution,
135 Ershadi et al. (2015) provided a more focused analysis on the influence of model structure and
136 resistance parameterization on single, two-layer and three-source Penman-Monteith models.
137 The authors identified considerable variability in the performance of models due to their
138 structure and parameterization choices.

139 While establishing a baseline level of performance at the tower scale is important,
140 understanding the impact of using the large-scale globally-gridded forcing that will ultimately
141 drive the global products is key. Indeed, undertaking a parallel assessment between the tower
142 and grid scales, while imposing consistency in the forcing data and sampling locations used,
143 allows for a much greater understanding of model response than can be achieved through

Matthew McCabe 5/1/2016 10:20 AM

Deleted: -

Matthew McCabe 5/1/2016 10:20 AM

Moved down [1]: A parallel effort to the LandFlux project is the European Space Agency (ESA) funded WAter Cycle Multi-mission Observation Strategy for EvapoTranspiration (WACMOS-ET; see <http://wacmoset.estellus.eu/>). WACMOS-ET, which is focused on an analysis period covering 2005-2007, seeks to better understand the impacts of model structure on flux estimation, with an additional focus on developing a consistent forcing dataset using predominantly European Space Agency developed products. A key result from these early works and the preliminary outcomes from WACMOS-ET support the finding that no single model or parameterization consistently outperformed any other across different biomes. Further details on these complimentary efforts can be found in Michel et al. (2015) and Miralles et al. (2015). -

165 [either assessment in isolation: an important extension upon recent tower-only analyses, such](#)
166 [as Ershadi et al. \(2014\) and related contributions.](#)

167 [A parallel effort to the LandFlux project is the European Space Agency \(ESA\) funded WAtEr](#)
168 [Cycle Multi-mission Observation Strategy for EvapoTranspiration \(WACMOS-ET; see](#)
169 <http://wacmoset.estellus.eu/>). WACMOS-ET, which is focused on an analysis period covering
170 [2005-2007, seeks to better understand the impacts of model structure on flux estimation, with](#)
171 [an additional focus on developing a consistent forcing dataset using predominantly European](#)
172 [Space Agency developed products. A key result from these early works and the preliminary](#)
173 [outcomes from WACMOS-ET support the finding that no single model or parameterization](#)
174 [consistently outperformed any other across different biomes. Further details on these](#)
175 [complimentary efforts can be found in Michel et al. \(2015\) and Miralles et al. \(2015\).](#)

176 The focus of the current investigation is to build upon these [recent](#) efforts as well as to
177 complement ongoing WACMOS-ET investigations, by simulating state-of-the-art evaporation
178 models using a joint assessment of tower-based meteorology and gridded data, and comparing
179 results with available eddy-covariance flux observations. Understanding how application of
180 gridded forcing data might influence the performance of the different models, relative to their
181 performance when forced with (presumably) higher-quality tower data, is a motivating
182 rationale for this work. Such evaluations are important [as they offer](#) insight into the sensitivity
183 of the models to input data uncertainties, provide a relative assessment of model quality and
184 also inform upon issues of spatial scale and footprint mismatch (McCabe and Wood, 2006).
185 Establishing model suitability for large-scale operational application as part of the GEWEX
186 Landflux project is a further motivating goal for this work. As such, a major objective is to
187 evaluate the individual model responses across a large range of biomes and climate zones. The
188 models selected for assessment include SEBS, PT-JPL, the Penman-Monteith based Mu model
189 (PM-Mu) (Mu et al., 2011) as well as the Global Land Evaporation Amsterdam Methodology
190 (GLEAM) (Miralles et al., 2011a). These models satisfy a number of criteria that were
191 considered important for global model selection, including reliance on a minimum number of
192 forcing variables, capacity to use remote sensing based observations, as well as previous
193 application at either the regional or global scale.

Matthew McCabe 5/1/2016 10:20 AM
Moved (insertion) [1]

Matthew McCabe 5/1/2016 10:20 AM
Deleted: past

Matthew McCabe 5/1/2016 10:15 AM
Deleted: in

Matthew McCabe 5/1/2016 10:16 AM
Deleted: developing

197

198 **2 Data and Methodology**

199 **2.1 Data**

200 For this analysis, model simulations cover the period from 1997 to 2007 and are performed at a
201 3-hourly temporal resolution. To examine model response and inter-product variability, a
202 parallel tower- and grid-based analysis was performed. Data for the tower-based analysis are
203 derived from a set of forty-five eddy-covariance towers (see Table A1), while the gridded data
204 are extracted from a compilation of available globally distributed satellite, meteorological and
205 land surface characteristics products. Compared to the 0.5 degree and 3-hourly gridded data,
206 the use of tower-based forcing is expected to minimize issues related to footprint uncertainties
207 when evaluating simulations against the observed eddy-covariance based flux data. The
208 primary purpose of the grid-based analysis is to better understand the effects of large-scale
209 forcing data on the accuracy of global retrievals, relative to the tower-based evaluations.

210 **2.1.1 Description of tower-based forcing data**

211 Data for the tower-based analyses are derived from forty-five eddy-covariance towers selected
212 from within the FLUXNET database (Baldocchi et al., 2001). [Table A1](#) lists the key attributes of
213 the selected towers and Figure A1 describes the varying temporal lengths of the tower records
214 used in this study. The requirement that towers only be used if they are able to provide the
215 input data required by all models (see Table 1) was a strong limiting criterion that significantly
216 reduced the number of available study sites. In particular, the availability of land surface
217 temperature data, which is required for SEBS, drastically constrained the choice of towers.
218 However, ensuring data consistency within the towers used for simulation and assessment was
219 an important component of this work, as it removes the impact of tower bias in subsequent
220 model assessment. Even with this reduced number, the selected towers represent a
221 considerable spatial spread encompassing a variety of biome types and climate zones (see
222 Figure 1).

Matthew McCabe 5/1/2016 10:57 AM

Deleted: Table A1

224 In terms of forcing data requirements, tower-based variables that were used for model
225 simulations include air temperature, relative humidity, wind speed, net radiation, ground heat
226 flux and precipitation. A summary of the forcing data requirements for each model is provided
227 in Table 1. Land surface emissivity, leaf area index and fractional vegetation cover were
228 estimated from Normalized Difference Vegetation Index (NDVI) data obtained from the Global
229 Inventory Monitoring and Modelling Study (GIMMS) dataset (Tucker et al., 2005), at 8 km
230 spatial and bi-monthly temporal resolutions. Here, the emissivity was calculated using the
231 approach of Sobrino et al. (2004), leaf area index was estimated following Fisher et al. (2008)
232 and the fractional vegetation cover was estimated using the technique described in Jiménez-
233 Muñoz et al. (2009). Land surface temperature was calculated using tower-observed longwave
234 upward radiation and by inverting the Stefan-Boltzmann equation (Brutsaert, 2005).
235 Atmospheric pressure data, which are absent from many towers, were calculated based on
236 ground elevation of tower locations using an equation presented in Bos et al. (2008). Canopy
237 height (h_c), which is needed for the SEBS model, was obtained from tower metadata and was
238 assumed constant during the simulation period. Although h_c varies over many vegetation types,
239 accounting for its within- and inter-annual variability is usually not possible, as observed data of
240 h_c variations are rarely recorded. Tower data were aggregated (i.e. summed for precipitation
241 and averaged for other input variables) from their native resolution of half-hourly or hourly to
242 3-hourly, to match the temporal resolution of the gridded data.

243 **2.1.2 Description of grid-based forcing data (LandFlux Version 0 forcing dataset)**

244 Grid-based data were developed by Princeton University for the LandFlux Version 0 (V-0)
245 dataset. The variables in the V-0 include air temperature, land surface temperature, wind
246 speed, atmospheric pressure, specific humidity, precipitation, net radiation, NDVI and leaf area
247 index. Net radiation data derive from the GEWEX Surface Radiation Budget (SRB) Version-3
248 (Stackhouse et al., 2011), while land surface temperature is determined by employing a
249 Bayesian post-processing procedure that merges High-Resolution Infrared Radiation Sounder
250 (HIRS) retrievals with the land surface temperature data from the National Centers for
251 Environment Prediction (NCEP) Climate Forecast System Reanalysis (CFSR) (Saha et al., 2010), as
252 described in Coccia et al. (2015). Precipitation data are also from the NCEP CFSR product and

253 have been bias-corrected to the Global Precipitation Climatology Project (GPCP) V2.2 dataset
254 (Adler et al., 2003). Likewise, atmospheric pressure, specific humidity and wind speed data
255 were extracted from the CFSR reanalysis data. For vegetation based parameters, NDVI data
256 were prepared by aggregating 8-km resolution GIMMS NDVI data to 0.5° resolution, while leaf
257 area index data were developed by Zhu et al. (2013) through fitting GIMMS NDVI data to the
258 Moderate Resolution Imaging Spectroradiometer (MODIS) MOD15A2 NDVI product, using a
259 neural network technique.

260 The majority of variables in the global LandFlux V-0 forcing dataset are at 0.5° spatial and 3-
261 hourly temporal resolution. Exceptions include the net radiation (1° and 3-hourly), NDVI (0.5°
262 and bi-monthly) and leaf area index (0.5° and monthly). For net radiation, the 1° data were
263 linearly interpolated to a 0.5° resolution. The bi-monthly NDVI data were assumed constant for
264 all 3-hourly time steps during each 15-day interval, while the leaf area index data were assumed
265 constant during each month. The canopy height over shrubland and forest biomes was
266 assumed fixed and was estimated using a static canopy height product developed by Simard et
267 al. (2011). For grassland and cropland biomes, where the dynamics of canopy height can be
268 considerable, canopy height was calculated using Equation 1, derived from Chen et al. (2012):

$$269 \quad h_c = h_c^{min} + \frac{h_c^{max} - h_c^{min}}{NDVI_{max} - NDVI_{min}} \times (NDVI - NDVI_{min}) \quad (1)$$

270 where h_c^{min} and h_c^{max} are the minimum and maximum canopy height and were obtained from
271 the static vegetation table of the North American Data Assimilation System (NLDAS) (available
272 from <http://ldas.gsfc.nasa.gov/nldas/web/web.veg.table.html>). $NDVI_{min}$ and $NDVI_{max}$ are the
273 minimum and maximum NDVI, respectively, and were calculated on a pixel-wise basis for each
274 calendar year. The JPL static vegetation height was aggregated linearly from 1 km to 0.5°.
275 Likewise, the NDVI derived canopy height was calculated at 8 km resolution and then
276 aggregated to 0.5°. Similar to the tower-based data, the methodology of Jiménez-Muñoz et al.
277 (2009) was used for the gridded forcing to estimate the fractional vegetation cover data from
278 NDVI data. The ground heat flux at the grid-scale was calculated as a fraction of net radiation
279 using fractional vegetation cover, following Su (2002).

280 **2.1.3 Model specific forcing data and data sources**

281 In addition to the data described above and shown in Table 1, both GLEAM and SEBS have some
282 model specific forcing data requirements. For SEBS, information on land surface temperature,
283 wind-speed and canopy height are required. At the tower-scale, these data are provided by
284 available meteorological forcing or meta-data descriptions in the case of canopy height. At the
285 grid-scale they are provided by a combination of the LandFlux V-O dataset and an adapted JPL
286 static vegetation height, as described in Section 2.1.2. GLEAM based simulations require
287 information on soil properties, vegetation optical depth (VOD), satellite soil moisture, snow
288 water equivalent, lightning frequency and vegetation cover fraction. Soil properties data for
289 GLEAM include field capacity, critical soil moisture and wilting point soil moisture thresholds.
290 Data for these were obtained from the Global Gridded Surfaces of Selected Soil Characteristics
291 dataset of the International Geosphere-Biosphere Programmes Data and Information System
292 (IGBP-DIS), available from Oak Ridge National Laboratory Distributed Active Archive Center
293 (<http://www.daac.ornl.gov>). Soil properties data were used in their native 5 arc-minute
294 resolution for tower-based analysis, but were aggregated to 0.5° for grid-based assessment.
295 Vegetation optical depth data was from Liu et al. (2011b) using a merged product from multiple
296 microwave based satellite data. The 0.25° spatial and daily temporal resolutions VOD data were
297 gap-filled as described by Miralles et al. (2011a). Soil moisture data assimilated in GLEAM
298 comes from the CCI-WACMOS dataset (Liu et al., 2012) produced from both active and passive
299 satellite microwave data at 0.25° and daily resolution. Snow water equivalent data are from the
300 GlobSnow product version 1.0 (Luojus et al., 2010); as GlobSnow covers the northern
301 hemisphere only, Global Monthly Snow Water Equivalent Climatology data from the National
302 Snow and Ice Data Center (NSIDC) (Armstrong et al., 2005) are used for the BW-Ma1 tower (see
303 [Table A1](#)) located in the southern hemisphere. Both GlobSnow data and the NSIDC product are
304 at approximately 0.25° spatial and daily temporal resolutions. Lightning frequency data is based
305 on the Combined Global Lightning Flash Rate Density monthly climatology at 0.5°(Mach et al.,
306 2007) and it is used to calculate a climatology of rainfall rates (Miralles et al., 2010). Finally,
307 vegetation cover fractions are derived from the MODIS MOD44B product (Hansen et al., 2005).
308 The MODIS continuous cover factions describe every pixel as a combination of its fractions of

Matthew McCabe 5/1/2016 10:57 AM
Formatted: Font:Not Italic, Check spelling and grammar
Matthew McCabe 5/1/2016 10:57 AM
Deleted: Table A1

310 water, tall canopy, short vegetation and bare soil. The temporal average of fractions is used
311 here for the MODIS period, providing only a static cover fraction for the GLEAM simulations.
312 The MOD44B product is available at 250 m and 0.25° resolution. For tower-based analysis,
313 cover fractions are at 250 m resolution, but for grid-based analysis the 0.25° MOD44B product
314 was aggregated to 0.5°.

315 Table 1 summarizes the different sources and spatio-temporal scales of the data that were used
316 for both the tower- and grid-based flux simulations. As noted earlier, the temporal analysis
317 encompasses the period 1997-2007, although as defined in Figure A1, the individual tower
318 records do not necessarily provide uninterrupted observations during this time range.

319 **2.1.4 Definition of selected biome type and climate zones**

320 The specific biomes examined in this work include wetland (WET), grassland (GRA), cropland
321 (CRO), shrubland (SHR), evergreen needleleaf forest (ENF), evergreen broadleaf forest (EBF) and
322 deciduous broadleaf forest (DBF). Biome type was specified in Fluxnet metadata records for
323 each of the individual tower sites and follows the International Geosphere-Biosphere
324 Programme (IGBP) classification. For simplicity, the shrubland biome is comprised of closed
325 shrubland, woody savannah and mixed forest biomes. The number of towers for each biome
326 type varies, with fourteen for evergreen needleleaf forest, ten for grassland, seven for
327 cropland, seven for deciduous broadleaf forest, four for shrubland, two for wetland and only
328 one for evergreen broadleaf forest (see Table A1). The climate zones include boreal (BOR), sub-
329 tropical (subTRO), temperate (TEMP), temperate-continental (TempCONT) and dry (DRY) for
330 arid and semi arid regions. These zones were prescribed from the tower specific metadata,
331 which were in turn derived from Rubel and Kottek (2010), based on a Köppen-Geiger climate
332 classification. As with biome type, the towers are not evenly distributed across climate zones,
333 with fifteen for temperate, eleven for sub-tropical, eight for temperate-continental, five for
334 boreal and six for dry regions (see Table A1).

335 **2.2 LandFlux Model Descriptions**

336 Following are brief descriptions of the models employed in this analysis. For a more
337 comprehensive explanation of the implementation of these different schemes, the reader is
338 referred to the principal model references as well as the recent contributions of Ershadi et al.
339 (2014) and Ershadi et al. (2015).

340 **2.2.1 SEBS**

341 SEBS is a widely employed process-based model used in the estimation of evaporation. The
342 model uses a variety of land surface and atmospheric variables and parameters for simulating
343 the transfer of heat and water vapor from the land surface to the atmosphere. To do so, the
344 model first estimates the representative roughness of the land surface and then uses roughness
345 parameters, temperature gradient and wind speed data to estimate sensible heat flux via a set
346 of flux-gradient equations describing the transfer of heat from the land surface to the
347 atmosphere. Depending on the atmospheric boundary layer height, the model uses either the
348 Monin-Obukhov Similarity Theory or the Bulk Atmospheric Similarity Theory equations
349 (Brutsaert, 2005). The model estimates the sensible heat flux of hypothetically wet and dry
350 conditions and uses these extreme-cases to calculate the evaporative fraction. Evaporation is
351 then calculated as a fraction of the available energy. The model requires accurate values of net
352 radiation, land surface temperature, air temperature, humidity, wind speed and vegetation
353 phenology to calculate surface fluxes. SEBS relaxes the need for parameterization of the surface
354 resistance, but is sensitive to aerodynamic resistance parameterization (Ershadi et al., 2013).
355 Further details on SEBS and its model formulation can be found in Su (2002).

356 **2.2.2 PT-JPL**

357 The PT-JPL model of evaporation uses a minimum of meteorological and remote sensing data
358 and has been employed in a number of studies to estimate regional and global scales flux
359 response (Fisher et al., 2008; Sahoo et al., 2011; Vinukollu et al., 2011b; Vinukollu et al., 2011a;
360 Badgley et al., 2015). A key characteristic of the model is the use of bio-physiological properties
361 of the land surface to reduce Priestley-Taylor potential evaporation to actual values. The PT-JPL

362 is a three source model in which the total evaporation is partitioned into soil evaporation (λE_s),
363 canopy transpiration (λE_t), and wet canopy evaporation (λE_i), i.e. $\lambda E = \lambda E_s + \lambda E_t + \lambda E_i$. The
364 model first partitions the total net radiation to soil and vegetation components and calculates
365 potential evaporation for soil, for canopy and for the wet canopy. The model then determines a
366 set of constraint multipliers to represent the impacts of green canopy fraction, relative wetness
367 of the canopy, air temperature, plant water stress and soil water stress on the evaporative
368 process. The model uses the constraint multipliers to reduce the potential evaporation to actual
369 values for each component of the system. PT-JPL does not calibrate or tune parameter values
370 and does not use wind speed data or parameterizations of the aerodynamic and surface
371 resistances. However, the model does require accurate estimates of optimum temperature
372 (T_{opt}) (Potter et al., 1993) for canopy transpiration. The optimum temperature is the air
373 temperature at the time of peak canopy activity, when the highest values of absorbed
374 photosynthetically active radiation and minimum values of vapour pressure deficit occur.
375 Further details of the PT-JPL model can be found in Fisher et al. (2008).

376 **2.2.3 PM-Mu**

377 The PM-Mu was expanded from a two-source Penman-Monteith implementation (Mu et al.,
378 2007) to a three-source version (Mu et al., 2011), which forms the basis behind the near real-
379 time estimation of global evaporation in the MOD16 product (Mu et al., 2013) (n.b. the PM-Mu
380 nomenclature used herein reflects an identical description used in Michel et al. (2015) and
381 Miralles et al. (2015), where it is referred to as PM-MOD). Evaporation in the PM-Mu model is
382 the sum of soil evaporation, canopy transpiration and evaporation of the intercepted water in
383 the canopy, i.e. ($\lambda E = \lambda E_s + \lambda E_t + \lambda E_i$). Estimation of evaporation for interception and
384 transpiration components is based on the Penman-Monteith equation (Monteith, 1965). Actual
385 soil evaporation is calculated using potential soil evaporation and a soil moisture constraint
386 function from the Fisher et al. (2008) ET model. This function is based on the complementary
387 hypothesis (Bouchet, 1963), which defines land-atmosphere interactions from air vapour
388 pressure deficit and relative humidity. Evaporation components are weighted based on the
389 fractional vegetation cover, relative surface wetness and available energy. Parameterization of

390 aerodynamic and surface resistances for each source is based on extending biome specific
391 conductance parameters from the stomata to the canopy scale, using vegetation phenology
392 and meteorological data. In contrast to the majority of Penman-Monteith type of models, the
393 PM-Mu does not require wind speed and soil moisture data for parameterization of resistances.
394 However, global application of the model requires consideration of the fact that resistance
395 parameters were calibrated against data from a set of eddy-covariance towers. One
396 consideration that may influence model simulations is that this parameterization approach was
397 developed at the daily-scale. However, both the present and also a recent related study
398 (Miralles et al. 2015) suggest no obvious impact for sub-daily application. Further details on
399 PM-Mu can be found in Mu et al. (2011) and Mu et al. (2013).

400 **2.2.4 GLEAM**

401 GLEAM (Miralles et al., 2011a) has been used not only in estimating global evaporation
402 (Miralles et al., 2011b) but also in detection and evaluation of heatwaves (Miralles et al.,
403 2014a), climate variability (Miralles et al., 2014b) and land-atmospheric feedbacks (Guilod et
404 al., 2015). Designed as a satellite data based model, GLEAM first estimates interception loss
405 using the analytical method of Gash (1979) and then applies the Priestley-Taylor equation to
406 calculate potential evaporation for soil and vegetation. Like PT-JPL, the model constrains the
407 potential evaporation values to actual values by applying a stress factor, although GLEAM is
408 based on different assumptions and encompasses both moisture availability in a multi-layered
409 soil system and vegetation water content inferred from vegetation optical depth data (Liu et al.,
410 2011b). In contrast to SEBS, PT-JPL and PM-Mu, the GLEAM model is equipped with routines to
411 quantify sublimation of snow-covered regions, to estimate open-water evaporation and to
412 assimilate remote sensing soil moisture data. Routine application of GLEAM is usually
413 performed in time-series mode, in which the model tracks the changes of soil moisture state
414 across time steps. Here, to allow application of the model at the tower-scale, gaps in the tower
415 data were filled by establishing correlation between the variables in tower- and grid-based
416 data. Simulated evaporation values were filtered from the analysis for these gap-filled periods.
417 Further details on GLEAM can be found in Miralles et al. (2011a;b).

418 2.3 Model Simulation and Analysis

419 The four selected models were forced with both tower- and grid-based data. The results were
420 then filtered for daytime-only periods, defined as when the shortwave downward radiation
421 exceeds 20 W.m^{-2} , to avoid issues associated with negative net radiation and night-time
422 condensation. The data were also filtered for rain events, for negative sensible and latent heat
423 flux observations, for low quality or gap-filled tower records, for frozen land surfaces and for
424 times in which air temperature was less than or equal to $0 \text{ }^\circ\text{C}$. The performance of the models
425 was evaluated for individual towers, for the collection of data from all towers, for towers
426 classified across biome types and for towers classified across climate zones.

427 To evaluate the skill of the models, we used traditional scatterplots and common statistical
428 metrics including the coefficient of determination (R^2), slope (m) and y-intercept (b) of the
429 linear regression, the root-mean-square difference ($RMSD$), relative error [$RE =$
430 $RMSD/\text{mean}(\lambda E_{obs})$] and the Nash-Sutcliffe Efficiency (NSE) (Nash and Sutcliffe, 1970). In
431 developing these performance metrics, simulated evaporation was compared with tower-
432 observed evaporation (λE_{obs}) that were corrected for non-closure using the energy residual
433 technique, as described in Ershadi et al. (2014). Scatterplots of matching percentiles (referred
434 to hereafter as percentile plots) of observed evaporation versus simulated values from the 1st
435 to 99th percentile increment were also used (Section 3.1). The 25th percentile (Q_{25}), median
436 (Q_{50}) and 75th percentile (Q_{75}) were used for further model assessment. To establish the
437 response of the models to water availability at individual tower sites, we calculated an aridity
438 index as $AI = P/E_p$, with P the annual precipitation (mm.yr^{-1}) and E_p the annual potential
439 evaporation (mm.yr^{-1}), calculated using a Priestley-Taylor equation and assuming an alpha-
440 coefficient of 1.26. LandFlux V-0 data (Section 2.1.2) at 3-hourly resolution were used to
441 calculate aridity index values and an average value was calculated to represent the state of
442 water availability at specific tower locations.

443

445 **3.1 Relative performance of the models when using tower-based and gridded data**

446 Figure 2 and Figure 3 show scatterplots, percentile plots and relevant statistical metrics of the
447 modelled evaporation for all of the available 3-hourly data records from across the forty-five
448 towers (representing 115,148 records in total). For the tower-based analysis (see Figure 2), PT-
449 JPL presents the best overall performance with lower model spread and an $RMSD = 61 \text{ W.m}^{-2}$,
450 $RE = 0.41$, $R^2 = 0.71$ and an $NSE = 0.65$. The model slightly underestimates evaporation, with a
451 slope of linear regression equal to 0.91 and with the majority of the percentile plot (up to Q_{75})
452 located just under the 1:1 line. When considering results across all towers, GLEAM presents
453 comparable statistical performance to PT-JPL, with an $RMSD = 64 \text{ W.m}^{-2}$, $RE = 0.43$ and an $NSE =$
454 0.62 . GLEAM tends to slightly underestimate evaporation, with the slope of linear regression
455 equal to 0.84 and with the percentile plot being located under the 1:1 line. SEBS generally
456 overestimates evaporation and has the lowest overall performance, with an $RMSD = 101 \text{ W.m}^{-2}$,
457 $RE = 0.68$ and $NSE = 0.24$, even though it has one of the highest R^2 values at 0.72. For PM-Mu,
458 the model tends to underestimate evaporation, resulting in an $RMSD = 78 \text{ W.m}^{-2}$, $RE = 0.52$
459 and an $NSE = 0.45$. Overall, the PT-JPL and GLEAM seem to present as more robust candidate
460 models for estimation of evaporation, at least in terms of their statistical response at the tower
461 scale. All models show a large spread around the fitted linear regression line. While the
462 summary statistics are useful metrics of performance, the inter-tower variability of the models
463 is an important element of this work and will be discussed further in the following sections.

464 The effect of using globally-gridded forcing data on the evaporation models is presented in
465 Figure 3. Apart from providing a direct evaluation on the accuracy of the global LandFlux
466 product, assessing flux response to a change in forcing aids in diagnosing the model sensitivity
467 to data uncertainties (which are inherent in any data product). Likewise, an indirect assessment
468 of the issue of footprint mismatch between the gridded data (0.5°) and the eddy-covariance
469 tower (hundreds of meters) can also be inferred. Figure 3 clearly shows that use of the grid-
470 based data reduces the performance of all models relative to the tower-based runs, with all
471 statistics degrading with a change in forcing resolution. SEBS displayed the largest sensitivity to

472 forcing data, with a 0.4 decrease in *NSE* and a 28 W.m^{-2} increase in *RMSD*. The sensitivity of PT-
473 JPL and GLEAM to the use of gridded data was lower, with both showing an approximately 0.3
474 decrease in *NSE* and around 22 W.m^{-2} increase in *RMSD* when assessing the grid-based analysis.
475 Overall, PM-Mu shows the lowest sensitivity to forcing, with a 0.26 decrease in *NSE* and 18
476 W.m^{-2} increase in *RMSD*, albeit presenting the lowest correlation and slope of linear regression
477 for all model responses.

478 Overall, these results confirm that all models display a relatively high sensitivity to changes in
479 the type and quality of input forcing data. While gridded forcing data are expected to have a
480 mismatch with the tower-based forcing due to their larger pixel (and footprint) sizes, this
481 spatial mismatch will impact all of the applied models, albeit to a lesser or greater extent,
482 depending on forcing data requirements. While spatial scale no doubt plays a major role in
483 decreasing model efficiencies at grid-scales, a key reason for the differences in tower- versus
484 grid-based results relates to internal inconsistencies within the gridded forcing data. For
485 instance, SEBS is known to be particularly sensitive to the temperature gradient between the
486 land surface and the atmosphere (van der Kwast et al., 2009; Ershadi et al., 2013). While the
487 temperature gradient at the tower scale is more reliable due to application of the tower-based
488 sensors for air temperature and land surface temperature, obtaining such consistency is harder
489 when different sources of forcing data are employed (see Section 2.1). Not surprisingly, results
490 also indicate that those models that use fewer inputs show lower sensitivity to changes in the
491 forcing. As such, any inconsistency between the tower and gridded data is likely to have less
492 influence on the PT-JPL, GLEAM and PM-Mu models than it will on SEBS, which in addition to
493 vegetation height, requires both land surface temperature and wind speed data: two variables
494 with considerable spatial variability. Disentangling the varying influence of model structural and
495 forcing data uncertainty requires focused attention and is examined further in the Discussion
496 section.

497 The large spread of data in the scatterplots indicates that there is considerable variability in the
498 performance of the models at individual towers, irrespective of whether tower or gridded data
499 are used. Of course, it may also be indicative of systematic biases in the in-situ data, which vary
500 from one tower to another and subsequently impact on model spread: however, this is non-

501 trivial to determine. To investigate the nature of this variability, we extend the analysis by
502 developing time series of R^2 , RE and NSE at 3-hourly resolution for individual tower locations, as
503 shown in Figure 4. To examine performance as a function of hydrological condition, the towers
504 are arranged by degree of increasing aridity, as determined by calculation of an aridity index
505 (see Section 2.3), with left-to-right representing the transition from wet-to-dry and describing
506 an aridity index varying between approximately 2 and 0.

507 From Figure 4 it can be observed that there is a general downward trend in both R^2 and NSE as
508 aridity increases, with a slight upward trend reflected in RE . In terms of R^2 , most of the models
509 (except for PM-Mu) show some consistency in performance until an aridity index of around 0.7,
510 wherein models start to diverge. Similar agreement is seen in the relative error plot, although
511 the outlier here is SEBS, which shows variable performance unrelated to aridity changes.
512 Examining the Nash-Sutcliffe efficiency allows for a clearer evaluation of model response to be
513 obtained. For this metric, PT-JPL and GLEAM display relatively good correspondence for most of
514 the towers, but start to diverge more regularly for aridity indices below 0.8. Overall, PT-JPL
515 presents a marginally better response than GLEAM, with higher values of NSE and R^2 and lowest
516 values of RE produced across the majority of towers. Similar results are expressed in Figure A2,
517 which presents the same tower based inter-comparison as in Figure 4, but for the grid-scale
518 model simulations.

519 From Figure 2 it was observed that SEBS presented the lowest values of NSE and highest values
520 of RE , while PM-Mu had the lowest values of R^2 . Highlighting the importance of examining a
521 range of statistical metrics, the R^2 values for SEBS are actually comparable to those of PT-JPL
522 and GLEAM, or even higher for a majority of towers that have an aridity index less than 0.7.
523 Inspection of individual tower-based scatterplots for each of the models (not shown) illustrated
524 that while the SEBS evaporation has a strong linear relationship with observed values for a
525 majority of towers, the linear regression line exhibits a large slope, indicating an overestimation
526 in SEBS predictions. Those towers that exhibit drops in NSE (and rise in RE) for the SEBS model
527 (e.g. DE-Tha, NL-Loo, US-Wrc, FR-Pue; see Table A1) are located mainly in shrubland and forest
528 biomes, suggesting a dependency of SEBS model performance that is tied to land surface
529 vegetation characteristics. Although statistical variations are evident in all models, the greater

530 response variability in SEBS is likely due to problems in simulating heat transfer within the
531 roughness sub-layer (RSL), which often forms over tall and heterogenous land surfaces
532 (Harman, 2012). We explore the issue of skill dependency of certain models to biome type and
533 climate zone in Sections 3.2 and 3.3.

534 As noted, Figure 4 shows a general decrease in the predictive skill in all models where towers
535 have an aridity index less than 0.7, but particularly so for PM-Mu and SEBS. These reductions
536 may in part be due to data uncertainties in tower observations that originate from the
537 advection of dry air into the tower footprint, or to a reduced capacity of the models to
538 reproduce the evaporative response when evaporation represents a small fraction of the total
539 available energy. Two towers at which all models display poor performance are IT-Noe and IL-
540 Yat (see Figure 1). It seems likely that IT-Noe is influenced by strong advection of moist air from
541 the Mediterranean Sea, while IL-Yat is influenced by advection of hot and dry air from
542 surrounding desert regions. None of the models in this study are able to specifically account for
543 advection and are thus prone to misrepresenting the observed evaporative response.

544 **3.2 Performance of the models across biomes**

545 The variability in model performance across the tower sites observed in Figure 4 and Figure A2,
546 indicates that a biome-specific assessment could be useful to determine whether the
547 performance of the models is also correlated to the underlying land cover, in addition to any
548 aridity influence. Figure 5 presents the R^2 , RE and NSE for each of the models for the seven
549 different biome classes. The analysis was conducted using the higher quality tower-based
550 simulations for all available 3-hourly data. One immediate highlight from Figure 5 is the
551 relatively poor performance of all models over shrubland sites, where low values of NSE (i.e.
552 $NSE \leq 0.05$) and reduced R^2 can be observed. Ershadi et al. (2014) observed a similarly poor
553 response over shrublands in a separate tower-based analysis that employed some of the same
554 models examined here. They attributed the result to difficulties in the parameterization of the
555 models over such landscapes due to the strong heterogeneities present in these environments,
556 as well as inherent water limitations. For instance, the capacity of the GIMMS NDVI data with 8

557 km spatial resolution is clearly insufficient in effectively parameterizing the roughness for SEBS,
558 resistances for PM-Mu and constraint functions for the PT-JPL.

559 Excluding shrublands from the analysis, the PT-JPL is one of the best performing models across
560 the remaining biomes, having the highest values of NSE and R^2 and lowest relative errors.
561 Consistency in the performance of PT-JPL across biome types has been reported in earlier
562 studies (Vinukollu et al., 2011a; Ershadi et al., 2014) and was variously ascribed to the
563 formulation of its constraint functions (see Section 2.2.2) and the minimal forcing data
564 requirements, which reduce its sensitivity to uncertainties in input data. GLEAM closely follows
565 PT-JPL for evergreen needleleaf forest and grassland biomes, but shows marginally lower NSE
566 values for other biomes. Figure 5 also indicates that while SEBS has relatively high values of R^2
567 over the majority of biome types, it fails to provide sufficient predictive skill for the estimation
568 of evaporation over shrublands and forest biomes. These biome types are characterized by tall
569 and heterogeneous canopies, within which the roughness sub-layer forms. The reduced
570 capacity of the SEBS flux gradient functions in simulating heat transfer within the roughness
571 sub-layer has been highlighted previously (Weligepolage et al., 2012; Ershadi et al., 2014).
572 Although performing poorly in shrubland and forest biomes, the SEBS model exhibits a
573 comparatively good performance across wetlands, grasslands and croplands, where shorter
574 canopies dominate. PM-Mu presents the lowest values of R^2 across all biomes, although the
575 model presents reasonable NSE values over cropland (0.64) and broadleaf forest (>0.54)
576 biomes. Improved performance of the PM-Mu model over croplands has been observed in a
577 recent study (Ershadi et al., 2015), but the key reasons for low R^2 values of the model across
578 other biomes is not immediately apparent and requires further investigation.

579 Percentile plots of the 3-hourly tower-based results were used to identify whether a model
580 under- or over-estimates evaporation across its distribution function. From Figure 6 it can be
581 seen that SEBS clearly overestimates while PM-Mu underestimates evaporation across all
582 biome types, reflecting those results presented in Figure 2. The percentile plots for SEBS are
583 close to the 1:1 line for grassland and cropland biomes that have short canopy height,
584 confirming the observations made for Figure 4 and Figure 5. PT-JPL shows good model
585 reproduction of observed values over grassland and deciduous broadleaf forest biomes, with

586 the percentile plots close to the 1:1 line. However, the model slightly underestimated
587 evaporation for croplands and overestimated evaporation for wetlands, with the tails
588 (percentiles greater than Q_{75}) reflecting greater divergence than the bulk of the distribution.
589 The rate of overestimation was higher for evergreen needleleaf forest, evergreen broadleaf
590 forest and for shrubland biomes. Figure 6 also shows that GLEAM presents strong performance
591 over grasslands, croplands and evergreen needleleaf forest sites, underestimated evaporation
592 across deciduous broadleaf forest sites and tended to overestimate evaporation across the
593 remaining biomes (wetlands, shrublands and evergreen broadleaf forests).

594 Overall, all models show a tendency towards reduced performance when applied over forest
595 biomes, but improved performance over shorter canopies. These results may be reflecting the
596 fundamental physical basis behind approaches such as the base Penman-Monteith (Penman,
597 1948), Priestley-Taylor (Priestley and Taylor, 1972) and Monin-Obukhov flux gradient functions,
598 which were developed for such surface types (Brutsaert, 1982), highlighting the challenges
599 inherent in global scale application of such models, especially over diverse land cover types.

600 To further evaluate the influence of biome type on evaporation estimation and to discriminate
601 the role of individual forcing variables in impacting model efficiencies, the NSE and R^2 values
602 between tower- and grid-based data were calculated for the flux response, as well as for key
603 forcing variables such as net radiation, land surface temperature, air temperature, wind speed,
604 specific humidity, fractional vegetation cover and leaf area index. As can be seen in Figure 7,
605 agreement between tower-based and grid-based net radiation data is relatively high across all
606 biomes, but especially so over forest biomes ($NSE \geq 0.67$). Grid-based wind speed data have the
607 most variable agreement with tower data, with R^2 and NSE values generally lower than other
608 selected variables across all of the examined biomes. Air temperature shows good agreement,
609 with both high NSE values ($NSE \geq 0.7$) and high R^2 values ($R^2 \geq 0.84$). Specific humidity data are
610 also well reproduced ($NSE \geq 0.72$), as is land surface temperature with an $NSE \geq 0.80$ for all
611 biomes. In sharing a common GIMMS-NDVI based derivation, the agreement for fractional
612 vegetation cover and leaf area index data is reasonable over the majority of biomes, except
613 over evergreen broadleaf forest, where both the R^2 and NSE are low.

614 The lower panel of Figure 7 show R^2 and NSE values for both the tower- and grid-based
615 simulations against eddy-covariance observations for each of the models, discriminated by
616 biome type. As can be seen, the performance of all models is reduced across all biomes when
617 grid-based forcing data is used, a result reflected in all cases by relatively lower NSE and R^2
618 values. PM-Mu had the smallest and SEBS had the largest decrease in performance over a
619 majority of the biomes, in accordance with the findings of Section 3.1. PT-JPL and PM-Mu had a
620 relatively constant decrease in NSE and R^2 for the grid-based simulations. Decreased modelling
621 performance was also maintained for GLEAM, except over the single evergreen broadleaf forest
622 tower, where a more significant departure (relative to the other biome types), was observed.
623 SEBS showed a much larger variability in performance reduction, with smaller variations due to
624 forcing over forest biomes and larger reductions over biomes with shorter canopies. The
625 significant decrease in NSE for SEBS over grassland, cropland and to some extent the wetland
626 biome, cannot be immediately associated with NSE or R^2 changes in any of the forcing variables.
627 It is interesting that the agreement over grassland and cropland biomes between tower- and
628 grid-based variables is amongst the highest (especially for wind speed, fractional vegetation
629 cover and for leaf area index data), yet the subsequent model performance is among the worst.
630 The use of global statistics to evaluate model response makes discriminating the cause of this
631 variability difficult. It is possible that the statistics are biased low due to the influence of one or
632 a few individual towers, by errors in the forcing fields driving model parameterizations (i.e.
633 vegetation height) or in response to model sensitivities to particular forcing variables. Either
634 way, these results highlight the difficulties in diagnosing the cause of performance response
635 and related sensitivity to forcing data variables in complex process-based models, which often
636 display a high degree of interactions between the variables. Indeed, diagnosing the forcing
637 variables responsible for reducing the efficiency of particular models is not feasible with a
638 simple correlation analysis of the input data fields, but requires a separate and focused
639 sensitivity analysis.

640 3.3 Performance of the Models over Climate Zones

641 Similar to the biome-wise analyses, an evaluation of the models was conducted across a
642 number of distinct climate zones, with R^2 , RE and NSE values for tower-based 3-hourly
643 evaporation estimations shown in Figure 8. Yet again, the results highlight the importance of
644 considering a range of evaluation metrics, as the models display some variability relative to the
645 statistical measure being employed. Overall, both PT-JPL and GLEAM maintain a consistently
646 good performance over the majority of climate zones, with PT-JPL expressing a slightly
647 improved response over all zones except temperate, where GLEAM shows an improved
648 simulation. In terms of R^2 , PM-Mu presents the lowest values overall, while SEBS exhibits high
649 values over the majority of climate zones, similar to the biome based analysis. However, SEBS
650 generally fails to reproduce the observed evaporation response, with high RE and low NSE . All
651 models have their best performance over the temperate-continental climate zone, with high
652 NSE and R^2 and low RE , which was followed closely by the temperate climate zone. The lowest
653 overall performance for all models corresponded to the dry climate zone, again reflecting the
654 aridity based results in Figure 4. As discussed in Section 3.1, data uncertainties due to the role
655 of advection in dry regions and difficulties in the accurate estimation when confronted with low
656 evaporative fractions are likely reasons behind such performance reductions in dry regions.

657 Figure 9 displays the corresponding percentile plots of model performance over the five
658 different climate zones. As can be seen, PT-JPL and GLEAM provide generally good performance
659 over all climate zones, although GLEAM slightly underestimates evaporation for temperate-
660 continental and boreal climate zones. SEBS overestimates relative to tower-based evaporation
661 across all biomes, while PM-Mu generally underestimates, except over temperate and
662 temperate-continental climate zones, for which the percentile plot of PM-Mu are relatively
663 close to the 1:1 line.

664 Similar to Figure 7, Figure 10 outlines the model response differentiated for the different
665 climate zones when using grid-based forcing data. As can be seen from the lower panel, the
666 simulation performance is reduced across all climate zones, relative to the tower data. In
667 particular, SEBS is significantly impacted across the majority of climate zones, with both a
668 reduction in NSE and R^2 , except over boreal forests. One possible reason for this smaller

669 variation over boreal forests could be due to lower surface-to-air temperature gradients over
670 forests, which contributes to smaller sensible heat fluxes and consequently larger evaporative
671 fraction values (in contrast to model performance over dry climates, where the temperature
672 gradient is large). Nevertheless, the relationship between uncertainty in individual variables and
673 the reduction of modelling performances is not able to be determined here. Further analysis
674 examining the sensitivity of individual models to their forcing is required.

675

676 **4 Discussion**

677 Understanding the role of model forcing in influencing simulation results, as well as examining
678 the impacts of biome type and climate zone on flux response, are important elements in the
679 development of robust globally-distributed evaporation products. The focus of this study was
680 on evaluating a set of process-based models, to support the development of globally
681 distributed and long term observations of surface fluxes as part of the GEWEX LandFlux project.
682 Overall, the PT-JPL and GLEAM models provided the most consistent performance, while PM-
683 Mu tended to underestimate and SEBS overestimate evaporation relative to the forty-five eddy-
684 covariance tower observations examined here. However, while statistical analysis allows a
685 pseudo-ranking of model performance, more detailed evaluation across towers, and biome and
686 climate types highlighted the considerable within-model variability in performance. Results also
687 demonstrated that changing the scale of input forcing data from tower- to grid-based reduced
688 the quality of model estimates in all cases, but especially for SEBS, where a sensitivity to
689 surface-air temperature gradients plays a strong role. In the following, we examine these
690 results and interpret any implications for large-scale global applications.

691 With its relatively simple modelling structure, PT-JPL performed consistently well relative to the
692 other models that have more complex structures and parameterization configurations. One
693 possible reason for this response may relate to the constraint functions of PT-JPL serving a wide
694 range of hydro-meteorological conditions, encompassing energy-limited (e.g. boreal climate) to
695 water-limited (e.g. dry climate) conditions. The good performance of PT-JPL was also observed
696 in a recent multi-model evaluation study, with a summary of the strengths and limitations of

697 the model presented in Ershadi et al. (2014). GLEAM also performed well, both at the tower
698 and at the grid-scale (see Figure 4 and Figure A2). Previous studies have shown that the model
699 is sensitive to the accuracy of precipitation data (Miralles et al., 2011b), as this determines the
700 partitioning of intercepted evaporation in the model and the root-zone soil moisture.
701 Unfortunately, testing for such sensitivities was not possible here, as both tower- and grid-
702 based records were filtered for rainfall events in post-processing steps, in response to the
703 limitation of eddy-covariance observations during such events.

704 In terms of the *NSE*, R^2 and *RE*, PM-Mu followed PT-JPL and GLEAM, with the model tending to
705 underestimate evaporation when applied to most of the tower- and grid-based records. While
706 reasons for this underestimation are not immediately clear, a recent study examining the
707 structure and parameterization of Penman-Monteith type models (Ershadi et al., 2015) showed
708 that the PM-Mu, which has a three-source structure, underperformed relative to a single-
709 source (Monteith, 1965) and a two-layer approach (Shuttleworth and Wallace, 1985) across all
710 studied biome types except croplands. An interesting aspect of Ershadi et al. (2015) was that
711 application of the canopy transpiration resistance scheme of the PM-Mu in those simpler
712 models improved their prediction skills. As such, the reduced performance of the PM-Mu
713 predictions might relate to underlying structural and parameterization issues in the model. As
714 the operational model behind the generation of the current MOD16 global evaporation product
715 (Mu et al., 2013), further studies to diagnose the cause of these responses are required.

716 Regarding assessment against the tower-based eddy-covariance observations, SEBS performed
717 relatively poorly in most statistical metrics when compared to the other models, as it
718 overestimated evaporation across a majority of studied biomes and climate zones, except over
719 grasslands and cropland sites with short canopies (e.g. less than 3 m). Interestingly, even
720 though generally over-predicting results, it had one of the highest R^2 values, indicating good
721 correlation with the eddy-covariance observations. Findings from Ershadi et al. (2014) confirm
722 the good performance of the model over short canopies and its lack of performance over
723 shrublands and forests. In terms of performance against underlying biome type, it was
724 observed that any performance reduction was observed mainly across shrublands and forest
725 biomes, where the roughness sub-layer forms above the canopy (Harman, 2012). Importantly,

726 the flux-gradient functions of the SEBS model are not parameterized to effectively simulate the
727 heat transfer process in the roughness sub-layer, and hence the model fails to perform well
728 (Weligepolage et al., 2012). The reliance of SEBS on an accurate representation of the surface-
729 air temperature gradient also limits the effectiveness of the model for global application,
730 demanding improvements in characterizing the spatial and temporal representativeness of such
731 variables.

732 It is apparent from Sections 3.2 and 3.3 that the application of gridded data for modelling
733 evaporation inevitably reduces the predictive performance of all models, regardless of their
734 complexity in the evaporation process or their economy in forcing data requirements. In fact,
735 the footprint mismatch between the tower- and grid-based simulations is likely to increase
736 uncertainties in the forcing data and cause discrepancies between the simulated and tower-
737 based evaporation values. Importantly, comparing the models for their relative performance
738 (see Figure 7 and Figure 10) reveals that the performance decrease for grid-based analysis was
739 not equal amongst all of the models. For instance, SEBS was observed to be more sensitive to
740 the use of gridded forcing data, most likely as a result of inconsistencies in temperature
741 gradient fields: an aspect that has been noted previously (van der Kwast et al., 2009; Ershadi
742 et al., 2013). Although input uncertainty also impacts the performance of PT-JPL, PM-Mu and
743 GLEAM, the *NSE* and R^2 of gridded simulations for those models are closer to their tower-based
744 counterparts. Apart from indicating a robust model structure, the reduced impact seen in these
745 schemes may also be a consequence of avoiding the use of forcing data such as land surface
746 temperature and wind speed data, which are known to be uncertain at both the grid and
747 tower-scale. Regardless of the culprit behind the observed performance discrepancy between
748 tower and grid-based simulations, it is clear that some models are better suited to global
749 application than others – at least given the quality of currently available global forcing datasets.

750 Importantly, the results presented in Sections 3.2 and 3.3 showed that evaluating tower or grid-
751 based statistical responses alone is not enough to identify those forcing variables most
752 impacting model performance. Diagnosing forcing sensitivity is not trivial given non-linearities
753 in the models and the high level of interaction within model variables and parameters. Indeed,
754 caution is warranted in any approaches seeking to evaluate evaporation models using gridded

755 data in isolation, as this is likely to yield unreliable performance metrics of the models. It is
756 important to perform a parallel tower-based data assessment to increase confidence in any
757 single models performance (Su et al., 2005) in any evaluation approach, particularly those
758 occurring at global scales.

759 Although the largest possible set of eddy-covariance towers and a common set of forcing data
760 was used to evaluate the different model simulations, there are still inevitable limitations in the
761 evaluations. Identifying such limitations is important not only for the current evaluations, but
762 also in guiding future contributions. One such example relates to the period of tower data used
763 for evaluation in this study (see Figure A1), as the data record length varies amongst the towers
764 and the data are not uniformly distributed across seasons. Moreover, the towers are not evenly
765 distributed across the studied biomes and climate zones (see Figure 1, Table A1), with only one
766 tower covering the entire evergreen broadleaf forest biome and two towers covering the
767 wetland biome. Further, no towers were available for use in arctic and tropical climate zones.
768 Although the tropical climate zone, especially Amazonian forests, is accounted as a critical
769 component in studies of the global water and energy cycles (Chahine, 1992; Wohl et al., 2012),
770 relatively few towers in this zone provide land surface temperature and longwave upward
771 radiation data needed for the SEBS model. An additional limitation is the coarse (8 km) spatial
772 resolution of the GIMMS NDVI data used in the models for the tower-based analysis, as this
773 resolution certainly does not correspond with the footprint of eddy-covariance sensors at any
774 of the towers. Developments towards improving the availability and access to long-term high-
775 resolution Landsat images (e.g. via Google Earth Engine; <https://earthengine.google.org>) might
776 be one way to improve model forcing and evaluation exercises, especially with the
777 development of high-resolution vegetation products (Houborg et al. 2016).

778 While the accuracy of individual variables in the LandFlux dataset were enhanced by bias
779 correction against independent data sources (see Section 2.1), diagnosing the internal
780 consistency of the data fields (McCabe et al., 2008), especially for air temperature, land surface
781 temperature, wind speed and humidity, is a concept that has not received much attention to
782 date and demands more considered investigations and analysis. Internal consistency is an
783 extremely challenging objective, but is critically important for flux estimation, where so many

784 different forcing data are required. Essentially it demands that all required model data are
785 derived from a common set of forcing variables, rather than by the standard approach of
786 compilation based on availability and accessibility. The most illustrative example would be in
787 the development of radiation data, derived here from NASA-GEWEX SRB sources (Stackhouse et
788 al., 2011). Calculation of radiation components requires air temperature, surface temperature,
789 land surface and vegetation features, as well as numerous other elements. However, these
790 underlying variables are rarely if ever retained to provide a consistent overall forcing data set
791 (i.e. the meteorological variables used in producing the SRB data are not subsequently used to
792 drive the models). Interdependencies in forcing affect many variables in the estimation of
793 evaporation, yet products are not developed with this simple consistency principle in mind.
794 Apart from introducing further biases and uncertainties into model simulations, until such
795 consistency is attained, discriminating between the impact of forcing versus the model
796 sensitivity to that forcing will remain extremely challenging.

797 From one perspective, the performance of the evaporation models examined here seems
798 relatively poor, even when they are forced with high-quality tower-based data. PT-JPL, which
799 was identified as one of the most consistent and best performing models, still presented a
800 relative error of 41%, with errors for GLEAM, PM-Mu and SEBS of 43%, 52% and 72%,
801 respectively. However, it is important to recognise that tower-based evaluation represents one
802 of the strictest measure of model performance and comes with its own caveats. One question
803 that remains unanswered is whether it is even appropriate to expect models run with large-
804 scale gridded forcing to replicate the small-scale response observed by eddy-covariance towers.
805 The alternative perspective, given inherent uncertainties in forcing, observations and
806 specification of model parameters, is that these results are encouraging. Broader scale metrics
807 such as hydrological consistency (McCabe et al., 2008), catchment based assessments or water
808 budget closure approaches would provide a better guide (Sheffield et al., 2009) and indeed,
809 such evaluations will need to be performed. These questions highlight the difficulties in not just
810 producing global estimates, but perhaps more importantly, in evaluating their quality.

811 The observed variability of modelling performance across the studied biomes and climate zones
812 implies that caution is required in advocating any single model for large-scale or global

813 application. These results are consistent with previous findings undertaken across a smaller
814 number of towers and biome and climate types, that any one modelling approach is incapable
815 of accurately reflecting the range of flux responses occurring across diverse landscapes (Ershadi
816 et al., 2014; Ershadi et al., 2015). One possible solution to address this inherent model
817 limitation is to assemble a mosaicked product based on the predictive skill of the model(s) over
818 particular biomes or climate zones. Another approach might be to develop an ensemble
819 product using a suitable multi-model blending technique, such as a Bayesian Model Averaging
820 approach (Hoeting et al., 1999; Yao et al., 2014). Either way, it is clear that further multi-model
821 assessments are required for progressing global scale flux characterisation and to ensure a
822 robust and representative product is developed.

823

824 5 Conclusions

825 It is something of a contradiction that the global-scale estimation of surface fluxes is both
826 straightforward and extremely challenging at the same time. It is more straightforward than
827 ever due to the availability of needed forcing data from various sources, such as numerical
828 weather prediction or other operational products, as well as the increased development of
829 global satellite based datasets. However, the comparative ease with which products can be
830 developed belies the difficulties in actually developing robust and coherent simulations.
831 Uncertainties in the use of internally inconsistent forcing data, the influence of untested model
832 parameterizations over different land surface and climate types, violation of model
833 assumptions in their graduation from the local scale to global scale and the perennial question
834 on how to best evaluate model output all seek to confound global flux efforts.

835 The evaluation of four process-based evaporation models as part of the GEWEX LandFlux
836 project undertaken here over a range of biome types and climate zones, highlighted the
837 variable performance and verified the sentiment that no single model is able to consistently
838 outperform any other. While individual model results at the tower scale allowed for a relative
839 performance ranking, the overall model errors when considered globally were high. Of those
840 models assessed here and being considered as potential candidates for a GEWEX LandFlux

Matthew McCabe 5/1/2016 9:49 AM

Deleted: reflect

Matthew McCabe 5/1/2016 9:49 AM

Deleted:

843 product, PT-JPL and GLEAM represent the most likely schemes for providing consistent
844 simulation response over a range of biome and climate types. In a challenge for the
845 development of more accurate global flux products, application of gridded data reduces the
846 performance of all models, even if the overall performance ranking does not change between
847 simulation runs. Such a response has obvious implications when model simulations at the
848 continental and global scales are increasingly required in many applications and where not only
849 the forcing data have large uncertainties, but also the underlying assumptions of the models
850 themselves are likely to be questioned. Further investigations on the reasons for such variable
851 performance and ways to offset the inherent uncertainties in global forcing are required.
852 Additional research is also needed to improve the structure and parameterization of some of
853 these candidate models, to understand model sensitivities to forcing (by conducting a thorough
854 sensitivity analysis) and to develop and implement an appropriate ensemble modelling and
855 merging technique that takes advantage of individual model performance over defined regions.
856 Further detailed comparisons against estimates from more complex modelling systems, such as
857 reanalysis and numerical weather prediction models, are needed to provide greater context
858 and additional benchmarking metrics to guide future investigations.

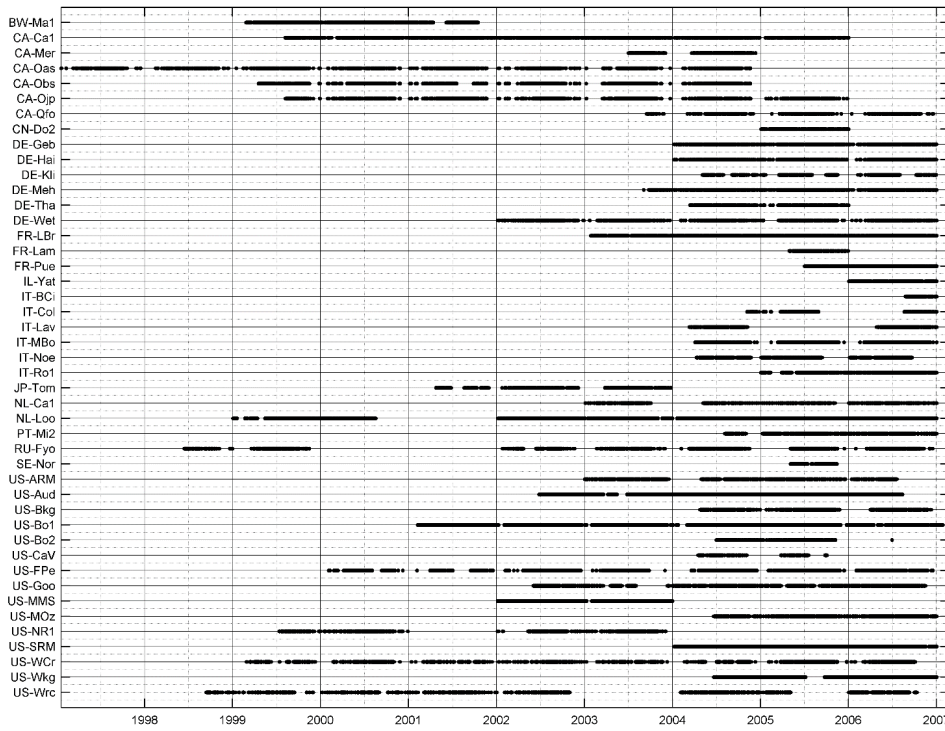
859 **Appendix A: Description of Tower Locations**

860 Table A1: Selected eddy-covariance and their attributes. Further details and information on
861 individual tower sites can be found via the Fluxnet data portal (<http://fluxnet.fluxdata.org/>)

Site-ID	Country	Lat.	Lon.	Ground Elev. (masl)	Tower height (m)	IGBP	Climate Class	Climate Zone	Reference
BW-Ma1	Botswana	-19.9	23.6	947	12.6	WSA	BSh	Dry	(Veenendaal et al., 2004)
CA-Ca1	Canada	49.9	-125.3	324	43	ENF	Cfb	Temperate	(Humphreys et al., 2006)
CA-Mer	Canada	45.4	-75.5	68	3	WET	Dfb	Temperate-Continental	(Kross et al., 2013)
CA-Oas	Canada	53.6	-106.2	594	39	DBF	Dfc	Boreal	(Fu et al., 2014)
CA-Obs	Canada	54.0	-105.1	593	25	ENF	Dfc	Boreal	(Fu et al., 2014)
CA-Ojp	Canada	53.9	-104.7	517	28	ENF	Dfc	Boreal	(Hilton et al., 2014)
CA-Qfo	Canada	49.7	-74.3	389	25	ENF	Dfc	Boreal	(Flanagan et al., 2012)
CN-Do2	China	31.6	121.9	4	5	WET	Cfa	Sub-Tropical	(Yan et al., 2008)
DE-Geb	Germany	51.1	10.9	159	6	CRO	Cfb	Temperate	(Smith et al., 2010)

Site-ID	Country	Lat.	Lon.	Ground Elev. (masl)	Tower height (m)	IGBP	Climate Class	Climate Zone	Reference
DE-Hai	Germany	51.1	10.5	458	43.5	DBF	Cfb	Temperate	(Rebmann et al., 2005)
DE-Kli	Germany	50.9	13.5	480	3.5	CRO	Cfb	Temperate	(Smith et al., 2010)
DE-Meh	Germany	51.3	10.7	289	3	GRA	Cfb	Temperate	(Don et al., 2009)
DE-Tha	Germany	51.0	13.6	387	42	ENF	Cfb	Temperate	(Delpierre et al., 2009)
DE-Wet	Germany	50.5	11.5	789	27	ENF	Cfb	Temperate	(Richardson et al., 2010)
FR-LBr	France	44.7	-0.8	71	41	ENF	Cfb	Temperate	(Göckede et al., 2008)
FR-Lam	France	43.5	1.2	182	3.65	CRO	Cfb	Temperate	(Merlin et al., 2011)
FR-Pue	France	43.7	3.6	271	13	EBF	Csa	Sub-Tropical	(Soudani et al., 2014)
IL-Yat	Israel	31.3	35.1	654	18	ENF	BSh	Dry	(Sprintsin et al., 2011)
IT-BCi	Italy	40.5	15.0	9	2	CRO	Csa	Sub-Tropical	(Reichstein et al., 2003)
IT-Col	Italy	41.8	13.6	1534	25	DBF	Cfa	Sub-Tropical	(Chiti et al., 2010)
IT-Lav	Italy	46.0	11.3	1367	33	ENF	Cfb	Temperate	(Stoy et al., 2013)
IT-MBo	Italy	46.0	11.0	1563	2.5	GRA	Cfb	Temperate	(Gamon et al., 2010)
IT-Noe	Italy	40.6	8.2	27	3.6	CSH	Csa	Sub-Tropical	(Carvalhais et al., 2010)
IT-Ro1	Italy	42.4	11.9	174	20	DBF	Csa	Sub-Tropical	(Chiti et al., 2010)
JP-Tom	Japan	42.7	141.5	133	42	MF	Dfb	Temperate-Continental	(Saigusa et al., 2010)
NL-Ca1	Netherlands	52.0	4.9	-1	5	GRA	Cfb	Temperate	(Gioli et al., 2004)
NL-Loo	Netherlands	52.2	5.7	34	27	ENF	Cfb	Temperate	(Sulkava et al., 2011)
PT-Mi2	Portugal	38.5	-8.0	191	2.5	GRA	Csa	Sub-Tropical	(Gilmanov et al., 2007)
RU-Fyo	Russia	56.5	32.9	274	29	ENF	Dfb	Temperate-Continental	(Smith et al., 2010)
SE-Nor	Sweden	60.1	17.5	35	103	ENF	Dfb	Temperate-Continental	(Zierl et al., 2007)
US-ARM	USA	36.6	-97.5	318	60	CRO	Cfa	Sub-Tropical	(Lokupitiya et al., 2009)
US-Aud	USA	31.6	-110.5	1474	4	GRA	BSk	Dry	(Horn and Schulz, 2011)
US-Bkg	USA	44.3	-96.8	496	4	GRA	Dfa	Temperate-Continental	(Hollinger et al., 2010)
US-Bo1	USA	40.0	-88.3	218	10	CRO	Dfa	Temperate-Continental	(Hollinger et al., 2010)
US-Bo2	USA	40.0	-88.3	220	10	CRO	Dfa	Temperate-Continental	(Hollinger et al., 2010)
US-CaV	USA	39.1	-79.4	993	4	GRA	Cfb	Temperate	(Hollinger et al., 2010)
US-FPe	USA	48.3	-105.1	632	3.5	GRA	BSk	Dry	(Horn and Schulz, 2011)
US-Goo	USA	34.3	-89.9	94	4	GRA	Cfa	Sub-Tropical	(Hollinger et al., 2010)
US-MMS	USA	39.3	-86.4	290	48	DBF	Cfa	Sub-Tropical	(Dragoni et al., 2011)
US-MOz	USA	38.7	-92.2	238	30	DBF	Cfa	Sub-Tropical	(Hollinger et al., 2010)
US-NR1	USA	40.0	-105.5	3053	26	ENF	Dfc	Boreal	(Hilton et al., 2014)
US-SRM	USA	31.8	-110.9	1120	6.4	WSA	BSk	Dry	(Cavanaugh et al., 2011)
US-WCr	USA	45.8	-90.1	524	30	DBF	Dfb	Temperate-Continental	(Curtis et al., 2002)
US-Wkg	USA	31.7	-109.9	1522	6.4	GRA	BSk	Dry	(Scott, 2010)

Site-ID	Country	Lat.	Lon.	Ground Elev. (masl)	Tower height (m)	IGBP	Climate Class	Climate Zone	Reference
US-Wrc	USA	45.8	-122.0	391	85	ENF	Csb	Temperate	(Wharton et al., 2009)

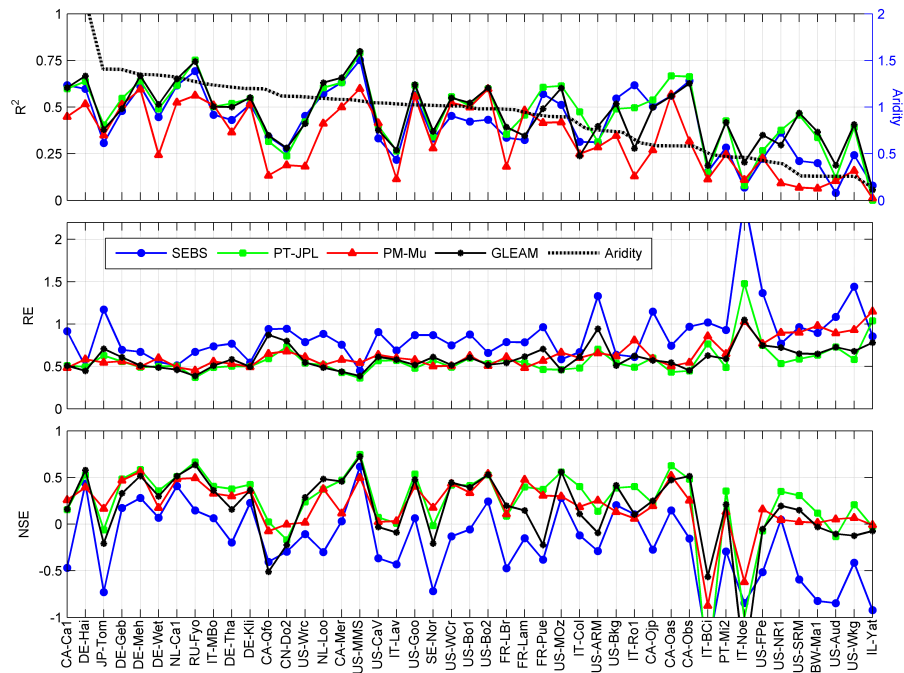


864

865 Figure A1: Temporal duration of the eddy-covariance based flux and tower meteorological
866 observations for each of the 45 sites used in this study

867

868



869

870 Figure A2: Comparison of the performance skill of the models in reproducing evaporation for
 871 the grid-based analyses. R^2 is the coefficient of determination, RE is relative error (lower is
 872 better) and NSE is the Nash-Sutcliffe Efficiency (higher is better). Towers are arranged from left
 873 to right based on an aridity index (secondary y-axis).

874

875 **Code Availability**

876 The PM-Mu, SEBS and PT-JPL models were coded in MATLAB as part of the GEWEX LandFlux and
877 WACMOS-ET projects, in discussion with (but independent of) the principal model authors, as
878 referenced in the relevant publications. The GLEAM model was developed in MATLAB by Diego Miralles
879 and Brecht Martens. All model code can be made available upon an emailed request to
880 hydrology@kaust.edu.sa, including a brief description of the intended purpose and application.

881 **Data Availability**

882 Evaporation model output presented here for both the gridded and tower based analyses can be
883 provided upon an emailed request to hydrology@kaust.edu.sa. The request should include a brief
884 description of the intended purpose and application of the model data.

885 **Acknowledgements**

886 Research reported in this publication was supported by the King Abdullah University of Science
887 and Technology (KAUST). D.G.M. acknowledges the financial support from The Netherlands
888 Organization for Scientific Research through grant 863.14.004. We appreciate the support of
889 the ESA funded WACMOS-ET project for both fruitful scientific discussions and guidance in
890 ensuring complementarity of these joint efforts. We thank the FLUXNET site investigators for
891 allowing the use of their meteorological data. This work used eddy-covariance data acquired by
892 the FLUXNET community and in particular by the AmeriFlux program (U.S. Department of
893 Energy, Biological and Environmental Research, Terrestrial Carbon Program: DE-FG02-
894 04ER63917 and DE-FG02-04ER63911), AfriFlux, AsiaFlux, CarboAfrica, CarboEuropeIP,
895 Carbotaly, CarboMont, ChinaFlux, Fluxnet-Canada (supported by CFCAS, NSERC, BIOCAP,
896 Environment Canada, and NRCan), GreenGrass, KoFlux, LBA, NECC, TCOS-Siberia, USCCC. We
897 acknowledge the financial support to the eddy-covariance data harmonization provided by
898 CarboEuropeIP, FAO-GTOS-TCO, iLEAPS, Max Planck Institute for Biogeochemistry, National
899 Science Foundation, University of Tuscia, Université Laval and Environment Canada and US
900 Department of Energy and the database development and technical support from Berkeley
901 Water Centre, Lawrence Berkeley National Laboratory, Microsoft Research eScience, Oak Ridge
902 National Laboratory, University of California - Berkeley, University of Virginia.

903

904 **References**

- 905 Adler, R. F., Huffman, G. J., Chang, A., Ferraro, R., Xie, P. P., Janowiak, J., Rudolf, B., Schneider, U., Curtis,
906 S., Bolvin, D., Gruber, A., Susskind, J., Arkin, P., and Nelkin, E.: The version-2 global precipitation
907 climatology project (GPCP) monthly precipitation analysis (1979-present), *Journal of*
908 *Hydrometeorology*, 4, 1147-1167, 2003.
- 909 Allen, R. G.: Using the FAO-56 dual crop coefficient method over an irrigated region as part of an
910 evapotranspiration intercomparison study, *Journal of Hydrology*, 229, 27-41, 2000.
- 911 Allen, R. G., Tasumi, M., and Trezza, R.: Satellite-Based Energy Balance for Mapping Evapotranspiration
912 with Internalized Calibration (METRIC)-Model, *Journal of Irrigation and Drainage Engineering*, 133,
913 380-394, 2007.
- 914 Armstrong, R. L., Brodzik, M. J., Knowles, K., and Savoie, M.: Global monthly EASE-Grid snow water
915 equivalent climatology, Boulder, CO: National Snow and Ice Data Center, Digital media, 2005.
916 2005.
- 917 Badgley, G., Fisher, J. B., Jiménez, C., Tu, K. P., and Vinukollu, R.: On uncertainty in global terrestrial
918 evapotranspiration estimates from choice of input forcing datasets, *Journal of Hydrometeorology*,
919 doi: 10.1175/JHM-D-14-0040.1, 2015. 2015.
- 920 Baldocchi, D., Falge, E., Gu, L., Olson, R., Hollinger, D., Running, S., Anthoni, P., Bernhofer, C., Davis, K.,
921 Evans, R., Fuentes, J., Goldstein, A., Katul, G., Law, B., Lee, X., Malhi, Y., Meyers, T., Munger, W.,
922 Oechel, W., Paw, K. T., Pilegaard, K., Schmid, H. P., Valentini, R., Verma, S., Vesala, T., Wilson, K.,
923 and Wofsy, S.: FLUXNET: A New Tool to Study the Temporal and Spatial Variability of Ecosystem-
924 Scale Carbon Dioxide, Water Vapor, and Energy Flux Densities, *Bulletin of the American*
925 *Meteorological Society*, 82, 2415-2434, 2001.
- 926 Bastiaanssen, W. G. M., Menenti, M., Feddes, R. A., and Holtslag, A. A. M.: A remote sensing surface
927 energy balance algorithm for land (SEBAL). 1. Formulation, *Journal of Hydrology*, 212-213, 198-
928 212, 1998.
- 929 Bos, M. G., Kselik, R. A. L., Allen, R. G., and Molden, D. J.: *Water Requirements for Irrigation and the*
930 *Environment*, Springer, Dordrecht, 2008.
- 931 Bouchet, R. J.: Evapotranspiration réelle et potentielle, signification climatique. General Assembly
932 Berkeley, International Association for Hydrological Sciences. Gentbrugge, Belgium. **62**: 134-142,
933 1963.

934 Brutsaert, W.: Evaporation Into the Atmosphere : theory, history, and applications, Reidel Publishing,
935 Dordrecht etc., 1982.

936 Brutsaert, W.: Hydrology : An Introduction, Cambridge University Press, Cambridge, 2005.

937 Brutsaert, W. and Stricker, H.: An advection-aridity approach to estimate actual regional
938 evapotranspiration, *Water Resour. Res.*, 15, 443-450, 1979.

939 Carvalhais, N., Reichstein, M., Collatz, G. J., Mahecha, M. D., Migliavacca, M., Neigh, C. S. R., Tomelleri,
940 E., Benali, A. A., Papale, D., and Seixas, J.: Deciphering the components of regional net ecosystem
941 fluxes following a bottom-up approach for the Iberian Peninsula, *Biogeosciences*, 7, 3707-3729,
942 2010.

943 Cavanaugh, M. L., Kurc, S. A., and Scott, R. L.: Evapotranspiration partitioning in semiarid shrubland
944 ecosystems: a two - site evaluation of soil moisture control on transpiration, *Ecohydrology*, 4,
945 671-681, 2011.

946 Chahine, M. T.: The hydrological cycle and its influence on climate, *Nature*, 359, 373-380, 1992.

947 Chen, X., Su, Z., Ma, Y., Yang, K., Wen, J., and Zhang, Y.: An Improvement of Roughness Height
948 Parameterization of the Surface Energy Balance System (SEBS) over the Tibetan Plateau, *Journal*
949 *of Applied Meteorology and Climatology*, 52, 607-622, 2012.

950 Chiti, T., Papale, D., Smith, P., Dalmonech, D., Matteucci, G., Yeluripati, J., Rodeghiero, M., and Valentini,
951 R.: Predicting changes in soil organic carbon in mediterranean and alpine forests during the Kyoto
952 Protocol commitment periods using the CENTURY model, *Soil use and management*, 26, 475-484,
953 2010.

954 Coccia, G., Siemann, A., Pan, M., and Wood, E. F.: Creating consistent datasets by combining remotely-
955 sensed data and land surface model estimates through Bayesian uncertainty post-processing: the
956 case of Land Surface Temperature from HIRS, *Remote Sensing of Environment*, 170, 290-305,
957 doi:10.1016/j.rse.2015.09.010, 2015.

958 Curtis, P. S., Hanson, P. J., Bolstad, P., Barford, C., Randolph, J. C., Schmid, H. P., and Wilson, K. B.:
959 Biometric and eddy-covariance based estimates of annual carbon storage in five eastern North
960 American deciduous forests, *Agricultural and Forest Meteorology*, 113, 3-19, 2002.

961 Delpierre, N., Soudani, K., Francois, C., Köstner, B., Pontailier, J. Y., Nikinmaa, E., Misson, L., Aubinet, M.,
962 Bernhofer, C., and Granier, A.: Exceptional carbon uptake in European forests during the warm
963 spring of 2007: a data–model analysis, *Global Change Biology*, 15, 1455-1474, 2009.

964 Don, A., Rebmann, C., Kolle, O., Scherer - Lorenzen, M., and Schulze, E. D.: Impact of afforestation -
965 associated management changes on the carbon balance of grassland, *Global Change Biology*, 15,
966 1990-2002, 2009.

967 Douville, H., Ribes, A., Decharme, B., Alkama, R., and Sheffield, J.: Anthropogenic influence on
968 multidecadal changes in reconstructed global evapotranspiration, *Nature Clim. Change*, 3, 59-62,
969 2013.

970 Dragoni, D., Schmid, H. P., Wayson, C. A., Potter, H., Grimmond, C. S. B., and Randolph, J. C.: Evidence of
971 increased net ecosystem productivity associated with a longer vegetated season in a deciduous
972 forest in south - central Indiana, USA, *Global Change Biology*, 17, 886-897, 2011.

973 Ershadi, A., McCabe, M. F., Evans, J. P., Chaney, N. W., and Wood, E. F.: Multi-site evaluation of
974 terrestrial evaporation models using FLUXNET data, *Agricultural and Forest Meteorology*, 187, 46-
975 61, 2014.

976 Ershadi, A., McCabe, M. F., Evans, J. P., Mariethoz, G., and Kavetski, D.: A Bayesian analysis of sensible
977 heat flux estimation: Quantifying uncertainty in meteorological forcing to improve model
978 prediction, *Water Resources Research*, 49, 2343-2358, 2013.

979 Ershadi, A., McCabe, M. F., Evans, J. P., and Wood, E. F.: Impact of model structure and parameterization
980 on Penman–Monteith type evaporation models, *Journal of Hydrology*, 525, 521-535, 2015.

981 Famiglietti, J. S., Lo, M., Ho, S. L., Bethune, J., Anderson, K. J., Syed, T. H., Swenson, S. C., de Linage, C. R.,
982 and Rodell, M.: Satellites measure recent rates of groundwater depletion in California's Central
983 Valley, *Geophysical Research Letters*, 38(3), 10.1029/2010GL046442, 2011.

984 Fisher, J. B., Tu, K. P., and Baldocchi, D. D.: Global estimates of the land-atmosphere water flux based on
985 monthly AVHRR and ISLSCP-II data, validated at 16 FLUXNET sites, *Remote Sensing of
986 Environment*, 112, 901-919, 2008.

987 Flanagan, L. B., Cai, T., Black, T. A., Barr, A. G., McCaughey, J. H., and Margolis, H. A.: Measuring and
988 modeling ecosystem photosynthesis and the carbon isotope composition of ecosystem-respired
989 CO₂ in three boreal coniferous forests, *Agricultural and Forest Meteorology*, 153, 165-176, 2012.

990 Fu, D., Chen, B., Zhang, H., Wang, J., Black, T. A., Amiro, B. D., Bohrer, G., Bolstad, P., Coulter, R., and
991 Rahman, A. F.: Estimating landscape net ecosystem exchange at high spatial–temporal resolution
992 based on Landsat data, an improved upscaling model framework, and eddy covariance flux
993 measurements, *Remote Sensing of Environment*, 141, 90-104, 2014.

994 Gamon, J. A., Coburn, C., Flanagan, L. B., Huemmrich, K. F., Kiddle, C., Sanchez-Azofeifa, G. A., Thayer, D.
995 R., Vescovo, L., Gianelle, D., and Sims, D. A.: SpecNet revisited: bridging flux and remote sensing
996 communities, *Can. J. Remote Sens.*, 36, S376-S390, 2010.

997 Gash, J. H.: An analytical model of rainfall interception by forests quarterly, *Journal of Royal*
998 *Meteorological Society*, 105, 43-45, 1979.

999 Gilmanov, T., Soussana, J., Aires, L., Allard, V., Ammann, C., Balzarolo, M., Barcza, Z., Bernhofer, C.,
1000 Campbell, C., Cernusca, A., Cescatti, A., Clifton-Brown, J., Dirks, B., Dore, S., Eugster, W., Fuhrer, J.,
1001 Gimeno, C., Gruenwald, T., Haszpra, L., Hensen, A., Ibrom, A., Jacobs, A., Jones, M., Lanigan, G.,
1002 Laurila, T., Lohila, A., Manca, G., Marcolla, B., Nagy, Z., Pilegaard, K., Pinter, K., Pio, C., Raschi, A.,
1003 Rogiers, N., Sanz, M., Stefani, P., Sutton, M., Tuba, Z., Valentini, R., Williams, M., and Wohlfahrt,
1004 G.: Partitioning European grassland net ecosystem CO₂ exchange into gross primary productivity
1005 and ecosystem respiration using light response function analysis, *Agriculture, Ecosystems and*
1006 *Environment*, 121, 93 - 120, 2007.

1007 Gioli, B., Miglietta, F., De Martino, B., Hutjes, R. W. A., Dolman, H. A. J., Lindroth, A., Schumacher, M.,
1008 Sanz, M. J., Manca, G., and Peressotti, A.: Comparison between tower and aircraft-based eddy
1009 covariance fluxes in five European regions, *Agricultural and Forest Meteorology*, 127, 1-16, 2004.

1010 Göckede, M., Foken, T., Aubinet, M., Aurela, M., Banza, J., Bernhofer, C., Bonnefond, J.-M., Brunet, Y.,
1011 Carrara, A., and Clement, R.: Quality control of CarboEurope flux data–Part 1: Coupling footprint
1012 analyses with flux data quality assessment to evaluate sites in forest ecosystems, *Biogeosciences*,
1013 5, 433-450, 2008.

1014 Granger, R. J.: Satellite-derived estimates of evapotranspiration in the Gediz basin, *Journal of Hydrology*,
1015 229, 70-76, 2000.

1016 Greve, P., Orłowsky, B., Mueller, B., Sheffield, J., Reichstein, M., and Seneviratne, S. I.: Global assessment
1017 of trends in wetting and drying over land, *Nature geoscience*, 7, 716-721, 2014.

1018 Guillod, B. P., Orłowsky, B., Miralles, D. G., Teuling, A. J., and Seneviratne, S. I.: Reconciling spatial and
1019 temporal soil moisture effects on afternoon rainfall, *Nat Commun*, 6, 2015.

1020 Hansen, M. C., Townshend, J. R. G., DeFries, R. S., and Carroll, M.: Estimation of tree cover using MODIS
1021 data at global, continental and regional/local scales, *Int. J. Remote Sens.*, 26, 4359-4380, 2005.

1022 Harman, I.: The Role of Roughness Sublayer Dynamics Within Surface Exchange Schemes, *Boundary-*
1023 *Layer Meteorology*, 142, 1-20, 2012.

1024 Hilton, T. W., Davis, K. J., and Keller, K.: Evaluating terrestrial CO₂ flux diagnoses and uncertainties from
1025 a simple land surface model and its residuals, *Biogeosciences*, 11, 217-235, 2014.

1026 Hirschi, M., Seneviratne, S. I., Alexandrov, V., Boberg, F., Boroneant, C., Christensen, O. B., Formayer, H.,
1027 Orłowsky, B., and Stepanek, P.: Observational evidence for soil-moisture impact on hot extremes
1028 in southeastern Europe, *Nature Geoscience*, 4, 17-21, 2011.

1029 Hoeting, J. A., Madigan, D., Raftery, A. E., and Volinsky, C. T.: Bayesian Model Averaging: A Tutorial,
1030 *Statistical Science*, 14, 382-401, 1999.

1031 Hollinger, D. Y., Ollinger, S. V., Richardson, A. D., Meyers, T. P., Dail, D. B., Martin, M. E., Scott, N. A.,
1032 Arkebauer, T. J., Baldocchi, D. D., and Clark, K. L.: Albedo estimates for land surface models and
1033 support for a new paradigm based on foliage nitrogen concentration, *Global Change Biology*, 16,
1034 696-710, 2010.

1035 Horn, J. E. and Schulz, K.: Identification of a general light use efficiency model for gross primary
1036 production, *Biogeosciences*, 8, 999 - 1021, 2011.

1037 Houborg, R., McCabe, M. F., and Gao, F.: A Spatio-Temporal Enhancement Method for medium
1038 resolution LAI (STEM-LAI), *International Journal of Applied Earth Observation and Geoinformation*,
1039 47, 15-29, 2016.

1040 Huffman, G. J., Adler, R. F., Rudolph, B., Schneider, U., and Keehn, P.: Global precipitation estimates
1041 based on a technique for combining satellite-based estimates, rain gauge analysis, and NWP
1042 model precipitation information, *J. Climate*, 8, 1284-1295, 1995.

1043 Humphreys, E. R., Black, T. A., Morgenstern, K., Cai, T., Drewitt, G. B., Nestic, Z., and Trofymow, J. A.:
1044 Carbon dioxide fluxes in coastal Douglas-fir stands at different stages of development after
1045 clearcut harvesting, *Agricultural and Forest Meteorology*, 140, 6-22, 2006.

1046 Jiménez, C., Prigent, C., Mueller, B., Seneviratne, S. I., McCabe, M. F., Wood, E. F., Rossow, W. B.,
1047 Balsamo, G., Betts, A. K., Dirmeyer, P. A., Fisher, J. B., Jung, M., Kanamitsu, M., Reichle, R. H.,

1048 Reichstein, M., Rodell, M., Sheffield, J., Tu, K., and Wang, K.: Global intercomparison of 12 land
1049 surface heat flux estimates, *J. Geophys. Res.*, 116, D02102, 2011.

1050 Jiménez-Muñoz, J., Sobrino, J., Plaza, A., Guanter, L., Moreno, J., and Martínez, P.: Comparison Between
1051 Fractional Vegetation Cover Retrievals from Vegetation Indices and Spectral Mixture Analysis:
1052 Case Study of PROBA/CHRIS Data Over an Agricultural Area, *Sensors*, 9, 768-793, 2009.

1053 Jung, M., Reichstein, M., Ciais, P., Seneviratne, S. I., Sheffield, J., Goulden, M. L., Bonan, G., Cescatti, A.,
1054 Chen, J., and de Jeu, R.: Recent decline in the global land evapotranspiration trend due to limited
1055 moisture supply, *Nature*, 467, 951-954, 2010.

1056 Kross, A., Seaquist, J. W., Roulet, N. T., Fernandes, R., and Sonnentag, O.: Estimating carbon dioxide
1057 exchange rates at contrasting northern peatlands using MODIS satellite data, *Remote Sensing of
1058 Environment*, 137, 234-243, 2013.

1059 Kustas, W. P., Perry, E. M., Doraiswamy, P. C., and Moran, M. S.: Using satellite remote sensing to
1060 extrapolate evapotranspiration in time and space over a semiarid rangeland, *Remote Sens.
1061 Environ.*, 49, 275-286, 1994.

1062 Liu, Y. Y., de Jeu, R. A. M., McCabe, M. F., Evans, J. P., and van Dijk, A. I. J. M.: Global long-term passive
1063 microwave satellite-based retrievals of vegetation optical depth, *Geophys. Res. Lett.*, 38, L18402,
1064 2011a.

1065 Liu, Y. Y., Dorigo, W. A., Parinussa, R. M., De Jeu, R. A. M., Wagner, W., McCabe, M. F., Evans, J. P., and
1066 Van Dijk, A. I. J. M.: Trend-preserving blending of passive and active microwave soil moisture
1067 retrievals, *Remote Sensing of Environment*, 123, 280-297, 2012.

1068 Liu, Y. Y., Parinussa, R. M., Dorigo, W. A., De Jeu, R. A. M., Wagner, W., Van Dijk, A. I. J., McCabe, M.
1069 F., and Evans, J. P.: Developing an improved soil moisture dataset by blending passive and active
1070 microwave satellite-based retrievals, *Hydrol. Earth Syst. Sci.*, 15, 425-436, 2011b.

1071 Liu, Y. Y., van Dijk, A. I. J. M., McCabe, M. F., Evans, J. P., and de Jeu, R. A. M.: Global vegetation biomass
1072 change (1988-2008) and attribution to environmental and human drivers, *Global Ecology and
1073 Biogeography*, 22, 692-705, 2013.

1074 Lokupitiya, E., Denning, S., Paustian, K., Baker, I., Schaefer, K., VERMA, S., MEYERS, T., Bernacchi, C. J.,
1075 SUYKER, A., and Fischer, M.: Incorporation of crop phenology in Simple Biosphere Model (SiBcrop)

1076 to improve land-atmosphere carbon exchanges from croplands, *Biogeosciences*, 6, 1103 - 1103,
1077 2009.

1078 Luojus, K., Pulliainen, J., Takala, M., Lemmetyinen, J., Derksen, C., and Wang, L.: Snow water equivalent
1079 (SWE) product guide, *Global Snow Monitoring for Climate Research*, 1, 2010.

1080

1081 Mach, D. M., Christian, H. J., Blakeslee, R. J., Boccippio, D. J., Goodman, S. J., and Boeck, W. L.:
1082 Performance assessment of the optical transient detector and lightning imaging sensor, *Journal of*
1083 *Geophysical Research: Atmospheres* (1984–2012), 112, 2007.

1084 McCabe, M. F. and Wood, E. F.: Scale influences on the remote estimation of evapotranspiration using
1085 multiple satellite sensors, *Remote Sensing of Environment*, 105, 271-285, 2006.

1086 McCabe, M. F., Wood, E. F., Wójcik, R., Pan, M., Sheffield, J., Gao, H., and Su, H.: Hydrological
1087 consistency using multi-sensor remote sensing data for water and energy cycle studies, *Remote*
1088 *Sensing of Environment*, 112, 430-444, 2008.

1089 Merlin, O., Al Bitar, A., Rivalland, V., Béziat, P., Ceschia, E., and Dedieu, G.: An analytical model of
1090 evaporation efficiency for unsaturated soil surfaces with an arbitrary thickness, *Journal of Applied*
1091 *Meteorology and Climatology*, 50, 457-471, 2011.

1092 Michel, D., Jiménez C., Miralles D. G., Jung M., Hirschi M., Ershadi A., Martens B., McCabe M. F., Fisher J.
1093 B., Mu Q., Seneviratne S. I., Wood E. F. and Fernández-Prieto D.: The WACMOS-ET project – Part
1094 1: Tower-scale evaluation of four remote sensing-based evapotranspiration algorithms, *Hydrol.*
1095 *Earth Syst. Sci. Discuss.*, 12(10): 10739-10787, 2015

1096 Miralles, D. G., De Jeu, R. A. M., Gash, J. H., Holmes, T. R. H., and Dolman, A. J.: Magnitude and variability
1097 of land evaporation and its components at the global scale, *Hydrol. Earth Syst. Sci.*, 15, 967-981,
1098 2011a.

1099 Miralles, D. G., Gash, J. H., Holmes, T. R. H., de Jeu, R. A. M., and Dolman, A.: Global canopy interception
1100 from satellite observations, *Journal of Geophysical Research*, 115, D16122, 2010.

1101 Miralles, D. G., Holmes, T. R. H., De Jeu, R. A. M., Gash, J. H., Meesters, A. G. C. A., and Dolman, A. J.:
1102 Global land-surface evaporation estimated from satellite-based observations, *Hydrol. Earth Syst.*
1103 *Sci.*, 15, 453-469, 2011b.

1104 Miralles, D. G., Teuling, A. J., van Heerwaarden, C. C., and de Arellano, J. V.-G.: Mega-heatwave
1105 temperatures due to combined soil desiccation and atmospheric heat accumulation, *Nature*
1106 *Geoscience*, 7, 345-349, 2014a.

1107 Miralles, D. G., van den Berg, M. J., Gash, J. H., Parinussa, R. M., de Jeu, R. A. M., Beck, H. E., Holmes, T.
1108 R. H., Jiménez, C., Verhoest, N. E. C., and Dorigo, W. A.: El Niño–La Niña cycle and recent trends in
1109 continental evaporation, *Nature Climate Change*, 4, 122-126, 2014b.

1110 Miralles, D. G., Jiménez C., Jung M., Michel D., Ershadi A., McCabe M. F., Hirschi M., Martens B., Dolman
1111 A. J., Fisher J. B., Mu Q., Seneviratne S. I., Wood E. F. and Fernández-Prieto D.: The WACMOS-ET
1112 project – Part 2: Evaluation of global terrestrial evaporation data sets, *Hydrol. Earth Syst. Sci.*
1113 *Discuss.*, 12(10): 10651-10700, 2015

1114 Monteith, J. L.: Evaporation and environment, *Symp. Soc. Exp. Biol.*, 19, 205-234, 1965.

1115 Mu, Q., Heinsch, F. A., Zhao, M., and Running, S. W.: Development of a global evapotranspiration
1116 algorithm based on MODIS and global meteorology data, *Remote Sensing of Environment*, 111,
1117 519-536, 2007.

1118 Mu, Q., Zhao, M., Kimball, J. S., McDowell, N. G., and Running, S. W.: A Remotely Sensed Global
1119 Terrestrial Drought Severity Index, *Bulletin of the American Meteorological Society*, 94, 83-98,
1120 2012.

1121 Mu, Q., Zhao, M., and Running, S. W.: Improvements to a MODIS global terrestrial evapotranspiration
1122 algorithm, *Remote Sensing of Environment*, 115, 1781-1800, 2011.

1123 Mu, Q., Zhao, M., and Running, S. W.: MODIS Global Terrestrial Evapotranspiration (ET) Product (NASA
1124 MOD16A2/A3), Algorithm Theoretical Basis Document, Collection, 5, 2013.

1125 Mueller, B., Hirschi, M., Jimenez, C., Ciais, P., Dirmeyer, P. A., Dolman, A. J., Fisher, J. B., Jung, M.,
1126 Ludwig, F., Maignan, F., Miralles, D., McCabe, M. F., Reichstein, M., Sheffield, J., Wang, K. C.,
1127 Wood, E. F., Zhang, Y., and Seneviratne, S. I.: Benchmark products for land evapotranspiration:
1128 LandFlux-EVAL multi-dataset synthesis, *Hydrol. Earth Syst. Sci. Discuss.*, 10, 769-805, 2013.

1129 Mueller, B., Seneviratne, S. I., Jimenez, C., Corti, T., Hirschi, M., Balsamo, G., Ciais, P., Dirmeyer, P.,
1130 Fisher, J. B., Guo, Z., Jung, M., Maignan, F., McCabe, M. F., Reichle, R., Reichstein, M., Rodell, M.,
1131 Sheffield, J., Teuling, A. J., Wang, K., Wood, E. F., and Zhang, Y.: Evaluation of global observations-

1132 based evapotranspiration datasets and IPCC AR4 simulations, *Geophysical Research Letters*, 38,
1133 2011.

1134 Nash, J. E. and Sutcliffe, J. V.: River flow forecasting through conceptual models: Part I - a discussion of
1135 principles, *Journal of Hydrology*, 10, 282-290, 1970.

1136 Nesbitt, S. W., Zipser, E. J., and Kummerow, C. D.: An examination of version-5 rainfall estimates from
1137 the TRMM Microwave Imager, precipitation radar, and rain gauges on global, regional, and storm
1138 scales, *J. Appl. Meteorol.*, 43, 1016-1036, 2004.

1139 Norman, J. M., Kustas, W. P., and Humes, K. S.: Source approach for estimating soil and vegetation
1140 energy fluxes in observations of directional radiometric surface temperature, *Agricultural and
1141 Forest Meteorology*, 77, 263-293, 1995.

1142

1143 Otkin, J. A., Anderson, M. C., Hain, C., and Svoboda, M.: Examining the Relationship between Drought
1144 Development and Rapid Changes in the Evaporative Stress Index, *Journal of Hydrometeorology*,
1145 15, 938-956, 2014.

1146 Penman, H. L.: Natural Evaporation from Open Water, Bare Soil and Grass, *Proceedings of the Royal
1147 Society of London. Series A. Mathematical and Physical Sciences*, 193, 120-145, 1948.

1148 Potter, C. S., Randerson, J. T., Field, C. B., Matson, P. A., Vitousek, P. M., Mooney, H. A., and Klooster, S.
1149 A.: Terrestrial ecosystem production: a process model based on global satellite and surface data,
1150 *Global Biogeochemical Cycles*, 7, 811-841, 1993.

1151 Priestley, C. H. B. and Taylor, R. J.: On the Assessment of Surface Heat Flux and Evaporation Using Large-
1152 Scale Parameters, *Mon. Weather Rev.*, 100, 81-92, 1972.

1153 Rebmann, C., Göckede, M., Foken, T., Aubinet, M., Aurela, M., Berbigier, P., Bernhofer, C., Buchmann,
1154 N., Carrara, A., and Cescatti, A.: Quality analysis applied on eddy covariance measurements at
1155 complex forest sites using footprint modelling, *Theor Appl Climatol*, 80, 121-141, 2005.

1156 Reichstein, M., Rey, A., Freibauer, A., Tenhunen, J., Valentini, R., Banza, J., Casals, P., Cheng, Y.,
1157 Grünzweig, J. M., and Irvine, J.: Modeling temporal and large - scale spatial variability of soil
1158 respiration from soil water availability, temperature and vegetation productivity indices, *Global
1159 biogeochemical cycles*, 17, 2003.

1160 Richardson, A. D., Black, T. A., Ciais, P., Delbart, N., Friedl, M. A., Gobron, N., Hollinger, D. Y., Kutsch, W.
1161 L., Longdoz, B., and Luyssaert, S.: Influence of spring and autumn phenological transitions on
1162 forest ecosystem productivity, *Philosophical Transactions of the Royal Society B: Biological*
1163 *Sciences*, 365, 3227-3246, 2010.

1164 Richey, A. S., Thomas, B. F., Lo, M.-H., Reager, J. T., Famiglietti, J. S., Voss, K., Swenson, S., and Rodell,
1165 M.: Quantifying renewable groundwater stress with GRACE, *Water Resources Research*, doi:
1166 10.1002/2015WR017349, 2015. n/a-n/a, 2015.

1167 Rubel, F. and Kottek M.: Observed and projected climate shifts 1901-2100 depicted by world maps of
1168 the Köppen-Geiger climate classification, *Meteorologische Zeitschrift*, 19(2): 135-141, 2010.

1169 Saha, S., Moorthi, S., Pan, H.-L., Wu, X., Wang, J., Nadiga, S., Tripp, P., Kistler, R., Woollen, J., and
1170 Behringer, D.: The NCEP climate forecast system reanalysis, *Bulletin of the American*
1171 *Meteorological Society*, 91, 1015-1057, 2010.

1172 Sahoo, A. K., Pan, M., Troy, T. J., Vinukollu, R. K., Sheffield, J., and Wood, E. F.: Reconciling the global
1173 terrestrial water budget using satellite remote sensing, *Remote Sensing of Environment*, 115,
1174 1850-1865, 2011.

1175 Saigusa, N., Ichii, K., Murakami, H., Hirata, R., Asanuma, J., Den, H., Han, S. J., Ide, R., Li, S. G., and Ohta,
1176 T.: Impact of meteorological anomalies in the 2003 summer on Gross Primary Productivity in East
1177 Asia, *Biogeosciences*, 7, 641-655, 2010.

1178 Scott, R. L.: Using watershed water balance to evaluate the accuracy of eddy covariance evaporation
1179 measurements for three semiarid ecosystems, *Agricultural and Forest Meteorology*, 150, 219-225,
1180 2010.

1181 Sheffield, J., Ferguson, C. R., Troy, T. J., Wood, E. F., and McCabe, M. F.: Closing the terrestrial water
1182 budget from satellite remote sensing, *Geophysical Research Letters*, 36, n/a-n/a, 2009.

1183 Sheffield, J., Wood, E. F., and Munoz-Arriola, F.: Long-term regional estimates of evapotranspiration for
1184 Mexico based on downscaled ISCCP data, *Journal of Hydrometeorology*, 11, 253-275, 2010.

1185 Shuttleworth, W. J. and Wallace, J. S.: Evaporation from sparse crops-an energy combination theory, *Q.*
1186 *J. R. Meteorol. Soc.*, 111, 839-855, 1985.

1187 Simard, M., Pinto, N., Fisher, J. B., and Baccini, A.: Mapping forest canopy height globally with
1188 spaceborne lidar, *Journal of Geophysical Research: Biogeosciences*, 116, G04021, 2011.

1189 Smith, P., Lanigan, G., Kutsch, W. L., Buchmann, N., Eugster, W., Aubinet, M., Ceschia, E., Béziat, P.,
1190 Yeluripati, J. B., and Osborne, B.: Measurements necessary for assessing the net ecosystem carbon
1191 budget of croplands, *Agriculture, ecosystems & environment*, 139, 302-315, 2010.

1192 Sobrino, J. A., Jiménez-Muñoz, J. C., and Paolini, L.: Land surface temperature retrieval from LANDSAT
1193 TM 5, *Remote Sensing of Environment*, 90, 434-440, 2004.

1194 Soudani, K., Hmimina, G., Dufrêne, E., Berveiller, D., Delpierre, N., Ourcival, J.-M., Rambal, S., and Joffre,
1195 R.: Relationships between photochemical reflectance index and light-use efficiency in deciduous
1196 and evergreen broadleaf forests, *Remote Sensing of Environment*, 144, 73-84, 2014.

1197 Sprintsin, M., Cohen, S., Maseyk, K., Rotenberg, E., Grünzweig, J., Karnieli, A., Berliner, P., and Yakir, D.:
1198 Long term and seasonal courses of leaf area index in a semi-arid forest plantation, *Agricultural and
1199 Forest Meteorology*, 151, 565-574, 2011.

1200 Stackhouse, P. W., Gupta, S. K., Cox, S. J., Zhang, T., Mikovitz, J. C., and Hinkelman, L. M.: The
1201 NASA/GEWEX surface radiation budget release 3.0: 24.5-year dataset, *GEWEX News*, 21, 10-12,
1202 2011.

1203 Stoy, P. C., Mauder, M., Foken, T., Marcolla, B., Boegh, E., Ibrom, A., Arain, M. A., Arneth, A., Aurela, M.,
1204 and Bernhofer, C.: A data-driven analysis of energy balance closure across FLUXNET research sites:
1205 The role of landscape scale heterogeneity, *Agricultural and forest meteorology*, 171, 137-152,
1206 2013.

1207 Su, H., McCabe, M. F., Wood, E. F., Su, Z., and Prueger, J. H.: Modeling evapotranspiration during
1208 SMACEX: Comparing two approaches for local- and regional-scale prediction, *Journal of
1209 Hydrometeorology*, 6, 910-922, 2005.

1210 Su, Z.: The Surface Energy Balance System (SEBS) for estimation of turbulent heat fluxes, *Hydrol. Earth
1211 Syst. Sci.*, 6, 85-100, 2002.

1212 Sulkava, M., Luyssaert, S., Zehle, S., and Papale, D.: Assessing and improving the representativeness of
1213 monitoring networks: The European flux tower network example, *Journal of Geophysical
1214 Research*, 116, 2011.

1215 Tucker, C. J., Pinzon, J. E., Brown, M. E., Slayback, D. A., Pak, E. W., Mahoney, R., Vermote, E. F., and El
1216 Saleous, N.: An extended AVHRR 8 - km NDVI dataset compatible with MODIS and SPOT
1217 vegetation NDVI data, *Int. J. Remote Sens.*, 26, 4485-4498, 2005.

1218 van der Kwast, J., Timmermans, W., Gieske, A., Su, Z., Oliosio, A., Jia, L., Elbers, J., Karssenber, D., and de
1219 Jong, S.: Evaluation of the Surface Energy Balance System (SEBS) applied to ASTER imagery with
1220 flux-measurements at the SPARC 2004 site (Barrax, Spain), *Hydrol. Earth Syst. Sci.*, 13, 1337-1347,
1221 2009.

1222 Veenendaal, M., Kolle, O., and Lloyd, J.: Seasonal variation in energy fluxes and carbon dioxide exchange
1223 for a broad leaved semi-arid savanna (Mopane woodland) in Southern Africa, *Global Change*
1224 *Biology*, 10, 318 - 328, 2004.

1225 Vinukollu, R. K., Sheffield, J., Wood, E. F., Bosilovich, M. G., and Mocko, D.: Multimodel Analysis of
1226 Energy and Water Fluxes: Intercomparisons between Operational Analyses, a Land Surface Model,
1227 and Remote Sensing, *Journal of Hydrometeorology*, 13, 3-26, 2011a.

1228 Vinukollu, R. K., Wood, E. F., Ferguson, C. R., and Fisher, J. B.: Global estimates of evapotranspiration for
1229 climate studies using multi-sensor remote sensing data: Evaluation of three process-based
1230 approaches, *Remote Sensing of Environment*, 115, 801-823, 2011b.

1231 Weligepolage, K., Gieske, A. S. M., van der Tol, C., Timmermans, J., and Su, Z.: Effect of sub-layer
1232 corrections on the roughness parameterization of a Douglas fir forest, *Agricultural and Forest*
1233 *Meteorology*, 162–163, 115-126, 2012.

1234 Wharton, S., Schroeder, M., Paw U, K. T., Falk, M., and Bible, K.: Turbulence considerations for
1235 comparing ecosystem exchange over old-growth and clear-cut stands for limited fetch and
1236 complex canopy flow conditions, *Agricultural and Forest Meteorology*, 149, 1477-1490, 2009.

1237 Wohl, E., Barros, A., Brunsell, N., Chappell, N. A., Coe, M., Giambelluca, T., Goldsmith, S., Harmon, R.,
1238 Hendrickx, J. M. H., Juvik, J., McDonnell, J., and Ogden, F.: The hydrology of the humid tropics,
1239 *Nature Clim. Change*, 2, 655-662, 2012.

1240 Yan, Y., Zhao, B., Chen, J., Guo, H., Gu, Y., Wu, Q., and Li, B.: Closing the carbon budget of estuarine
1241 wetlands with tower - based measurements and MODIS time series, *Global Change Biology*, 14,
1242 1690-1702, 2008.

1243 Yao, Y., Liang, S., Li, X., Hong, Y., Fisher, J. B., Zhang, N., Chen, J., Cheng, J., Zhao, S., and Zhang, X.:
1244 Bayesian multimodel estimation of global terrestrial latent heat flux from eddy covariance,
1245 meteorological, and satellite observations, *Journal of Geophysical Research: Atmospheres*, 119,
1246 4521-4545, 2014.

1247 Zhu, Z., Bi, J., Pan, Y., Ganguly, S., Anav, A., Xu, L., Samanta, A., Piao, S., Nemani, R. R., and Myneni, R. B.:
1248 Global data sets of vegetation leaf area index (LAI) 3g and Fraction of Photosynthetically Active
1249 Radiation (FPAR) 3g derived from Global Inventory Modeling and Mapping Studies (GIMMS)
1250 Normalized Difference Vegetation Index (NDVI3g) for the period 1981 to 2011, Remote Sensing, 5,
1251 927-948, 2013.

1252 Zierl, B., Bugmann, H., and Tague, C. L.: Water and carbon fluxes of European ecosystems: An evaluation
1253 of the ecohydrological model RHESSys, Hydrological processes, 21, 3328-3339, 2007.
1254

1255 Table 1: Summary of data sources for tower-based and grid-based analysis and their spatial and
 1256 temporal resolutions.

Variable	Tower-based	Grid-based	Model
Air temperature	Tower data aggregated to 3-hourly	LandFlux data at 0.5° and 3-hourly	All models
Humidity	Tower-based relative humidity converted to specific humidity and aggregated to 3-hourly	Specific humidity from LandFlux data at 0.5° and 3-hourly	All except GLEAM
Pressure	Calculated as a function of ground elevation	LandFlux data at 0.5° and 3-hourly	All models
Net radiation	Tower data aggregated to 3-hourly	LandFlux data from SRB v3 at 1° and 3-hourly	All models
Ground heat flux	Tower data aggregated to 3-hourly	Calculated from net radiation and fractional vegetation cover data, 0.5° and 3-hourly	All models
Land surface temperature	Calculated from tower-based longwave upward radiation and aggregated to 3-hourly	LandFlux data at 0.5° and 3-hourly	SEBS only
Wind speed	Tower data aggregated to 3-hourly	LandFlux data at 0.5° and 3-hourly	SEBS only
Canopy height	Tower meta data	JPL product and Equation 1	SEBS only
NDVI	GIMMS NDVI at 8km and bi-monthly	GIMMS NDVI at 0.5° and bi-monthly	All except GLEAM
Leaf area index	Calculated from NDVI	LandFlux data at 0.5° and monthly	SEBS and PM-Mu
Fractional vegetation cover	Not used as ground heat flux is available.	Calculated from NDVI	All except GLEAM
Precipitation	Tower data aggregated to 3-hourly	LandFlux data at 0.5° and 3-hourly	GLEAM only
Soil properties	IGBP-DIS at 5 arc-minutes	IGBP-DIS data aggregated to 0.5°	GLEAM only
Soil moisture	CCI-WACMOS data at 0.25° and daily	Same as tower-based	GLEAM only
Soil depth	GlobSnow (daily and 25 km)	Same as tower-based	GLEAM only
Vegetation optical depth	From Liu et al. (2011b) at 0.25° and daily	Same as tower-based	GLEAM only
Snow water equivalent	GlobSnow and NSIDC at 0.25° and daily	Same as tower-based	GLEAM only
Lightning frequency	Monthly climatology at 0.5°	Same as tower-based	GLEAM only
Cover fractions	MOD44B data at 250 m	MOD44B data at 0.5°	GLEAM only

1257

1258 Figure 1: Location of the selected towers and their distributions for various biomes

1259 Figure 2: Scatterplots of observed versus simulated latent heat flux for tower-based data.

1260 Colors show the frequency of values from high (red) to low (yellow). The thick black line
1261 represents the linear regression, while the thin line is the 1:1 line. The series of small circles
1262 show the percentile increments of data from the 1st to 99th, with large circles denoting the 25th,
1263 50th and 75th percentiles. The statistics shown on each figure provide coefficient of
1264 determination (R^2), slope (m), y-intercept (b), number of data records (n), the root-mean-
1265 squared difference (RMSE), relative error (RE) and the Nash-Sutcliffe Efficiency (NSE).

1266 Figure 3: Scatterplots of observed versus simulated evaporation for grid-based data. Colors

1267 show the frequency of values from high (red) to low (yellow). The thick black line is the linear
1268 regression and the thin line is the 1:1 line. The series of small circles show the percentile
1269 increments of data from the 1st to 99th, with large circles denoting the 25th, 50th and 75th
1270 percentiles. The statistics shown on the graphs are coefficient of determination (R^2), slope (m),
1271 y-intercept (b), number of data records (n), the root-mean-squared difference (RMSE), relative
1272 error (RE) and the Nash-Sutcliffe Efficiency (NSE).

1273 Figure 4: Comparison of the performance skill of the models in reproducing evaporation for the

1274 tower-based analyses. R^2 is the coefficient of determination, RE is relative error (lower is better)
1275 and NSE is the Nash-Sutcliffe Efficiency (higher is better). Towers are arranged from left to right
1276 based on an aridity index (secondary y-axis).

1277 Figure 5: Coefficient of determination (R^2), relative error (RE) and Nash-Sutcliffe Efficiency (NSE)

1278 for models across different biome types. Each point represents the collection of all available 3-
1279 hourly records of towers located within the selected biome, with the number of towers shown
1280 on the secondary y-axis of the R^2 plot in red. NSE for the shrubland response of SEBS is printed.

1281

1282 Figure 6: Percentile plots of observed (x-axis) versus estimated latent heat flux (y-axis) at 3-
1283 hourly resolution for the tower-based analysis across the seven studied biomes. Percentiles
1284 encompass the 1st to 99th range in 1 percent increments, with Q_{25} , Q_{50} and Q_{75} denoted by large
1285 coloured circles.

1286 Figure 7: The upper panel presents Nash-Sutcliffe Efficiency (NSE; x-axis) and R^2 (color tone)
1287 between tower- and grid-based values for net radiation, land surface temperature, air
1288 temperature, wind speed, specific humidity, fractional vegetation cover and leaf area index,
1289 across the seven studied biome types. The lower panel presents the NSE (x-axis) and R^2 of
1290 model simulated evaporation against closure-corrected observed values. The number of towers
1291 for each biome type used in the analysis are shown in red font on the secondary (right) axis in
1292 each of the plots. Statistics for those results beyond the range of the x-axis are printed
1293 separately on the plot.

1294 Figure 8: Coefficient of determination (R^2), relative error (RE) and Nash-Sutcliffe Efficiency (NSE)
1295 for model simulated results across the five different climate zones (y-axis). The zones are
1296 represented by dryland (DRY), temperate continental (TempCONT), temperate (TEMP), sub-
1297 tropical (subTRO) and boreal (BOR). Each point represents the collection of all towers located
1298 within the selected climate zone, with the number of towers shown on the secondary y-axis of
1299 the R^2 panel in red.

1300 Figure 9: Percentile plots of observed (x-axis) versus estimated latent heat flux (y-axis) at 3-
1301 hourly resolution for tower-based analysis and across the different climate zones. Percentiles
1302 encompass the 1st to 99th range in 1 percent increments. Q_{25} , Q_{50} and Q_{75} are denoted by large
1303 circles.

1304

1305

1306 Figure 10: The upper panel shows Nash-Sutcliffe Efficiency (NSE; x-axis) and R^2 (color tone)
1307 between tower-based and grid-based values for net radiation, land surface temperature, air
1308 temperature, wind speed, specific humidity, fractional vegetation cover and leaf area index
1309 across the five different climate zones. The lower panel shows NSE (x-axis) and R^2 of model
1310 simulated evaporation against closure-corrected observed values across climate zones. The
1311 number of towers for each biome are shown in red font on the secondary (right) axis of the
1312 plots. Statistics for the grid-based SEBS result over dry climate zone are printed.

1313

